Project Number: CYS-U539

The Use of Iron-oxide Nanoparticles for Hyperthermia Cancer Treatment and Simultaneous MRI Monitoring

A Major Qualifying Project

Submitted to the Faculty of

In partial fulfillment of the requirements for the

Degree of Bachelors of Science in Biomedical Engineering

By

Eileen Gribouski

Rafael Jaimes

April 30th, 2009

Advisor:

Professor C. Sotak, Ph.D.

Abstract

The overall goal of this project was to investigate the simultaneous use of magnetic iron-oxide nanoparticles (MNPs) for cancer treatment using hyperthermia as well as contrast agents that will allow MRI visualization of the particles within the tumor. Following characterization of the particles for use as both a therapeutic and MRI diagnostic agent, a strategy was designed for using MNPs in localized hyperthermia treatment of tumors; where MRI is used to both confirm the tumor uptake of the particles and as a tool to monitor the temperature changes in the tumor tissue during hyperthermia treatment.

TABLE OF CONTENTS

Authorship

The original material for each section was authored as follows:

Table of Figures

Table of Tables

I. Introduction

Magnetic Resonance Imaging (MRI) is a well-established clinical imaging modality for visualizing soft tissue in the body. MRI can be used alone or in conjunction with MRI contrast agents to enhance MR images. One class of MRI contrast agents is based on iron-oxide nanoparticles. In addition to their MRI contrast properties, iron-oxide nanoparticles can be used as an adjunct for killing cancerous tumor cells using hyperthermia. Hyperthermia is the process of heating tissue above normal physiological temperature. During hyperthermia, iron-oxide particles have the property that they can absorb and conduct heat more easily than body fluids and tissue alone. Iron-oxide particles can concentrate and conduct heat in an area that is specific to the location of the particles. In the case of cancers, the tumor vasculature is generally "leaky", allowing the particles to selectively concentrate in those regions as compared to healthy normal tissue. It is also important to note that the temperature to kill cancerous cells is lower than that of healthy cells. Consequently, using hyperthermia in conjunction with localized iron-oxide particles allows more heat to be selectively applied to the tumor; thus minimizing heat damage to the surrounding normal tissue. This project focuses on the development and characterization of iron-oxide nanoparticles for dual-use as: (1) a diagnostic MRI contrast agent that will allow MRI verification of tumor uptake of the particles; (2) a therapeutic adjunct to facilitate more effective localized heating of tumor tissue during hyperthermia.

To investigate the possibilities for using iron-oxide nanoparticles as dual-use diagnostic and therapeutic agents, a thorough literature review was performed to understand the wide range of potential applications for these agents. Following the literature review, an engineering design analysis was performed to determine the optimal conditions for image-guided hyperthermia using iron-oxide nanoparticles. As part of this project, the MRI and hyperthermia properties of the iron-oxide nanoparticles were characterized. Once this characterization was performed, the feasibility of using iron-oxide nanoparticles as dual-use diagnostic and therapeutic agents was evaluated.

Goal

The goal of this project is to characterize the MRI and hyperthermia properties of iron-oxide nanoparticles and then design and evaluate an optimal diagnostic/therapeutic strategy for the use of these agents for image-guided hyperthermia of tumors.

II. Literature Review

1. Magnetic Resonance Imaging (MRI)

i. MRI background information

Magnetic Resonance Imaging (MRI) has been used as a diagnostic tool in medicine for about thirty years and is based on the Nuclear Magnetic Resonance (NMR) technique. MRI uses a very strong magnetic field to polarize hydrogen nuclei (usually from water and fat) in the body; that is, the nuclei align themselves in either a "parallel" or "anti-parallel" orientation with respect to the main magnetic field direction. The polarized nuclei are then excited with a radiofrequency (RF) pulse; which is applied at a frequency specific to the nuclei and the strength of the main magnetic field. Immediately following the application of the RF pulse, the MRI signal is detected. The frequency and phase of the signal contains information about the spatial location of nuclei within the body. The MRI signal intensity is proportional to: (1) the number (concentration) of nuclei at a particular location in space; (2) the rate at which the nuclei re-align themselves in the main magnetic field following the RF excitation pulse – which is characterized by the T1 relaxation time; and (3) the rate of decay of the MRI signal itself during the signal-measurement period – which is characterized by the T2 relaxation time. Different tissues in a MR image are distinguished from one another based on differences in signal intensity that arise from differences in the concentration and T1 and T2 relaxation times of water protons in the respective tissues.

A schematic of a human MRI magnet assembly is shown in Figure 1 . The patient lies supine and is placed in the center of the magnet assembly. The magnet itself produces the main magnetic field along which the hydrogen atoms align. Within the MRI magnet assembly – also surrounding the patient – is radiofrequency (RF) coil which transmits RF pulses through the patient's body in order to excite the nuclei. After the RF pulse is turned off, the nuclei return to their initial equilibrium condition. During this process, an electrical current – proportional to the MRI signal – is induced into the same RF coil that was used to excite the nuclei in the first place. The MRI signal is digitized and – with subsequent digital signal processing – converted to the MR image. Also within the magnet assembly are a set of three magnetic field gradient coils. The geometry and relative orientation of these coils allow linear magnetic field gradients to be applied along the x, y, and z directions of a Cartesian co-ordinate frame within the magnet assembly. By applying current to the magnetic-field-gradient coils, the spatial location of nuclei within the patient can be encoded into the frequency and phase of the measured MRI signal.

Depending upon which magnetic-field-gradient coils are used, “sliced” images may be obtained from specific parts of the body.

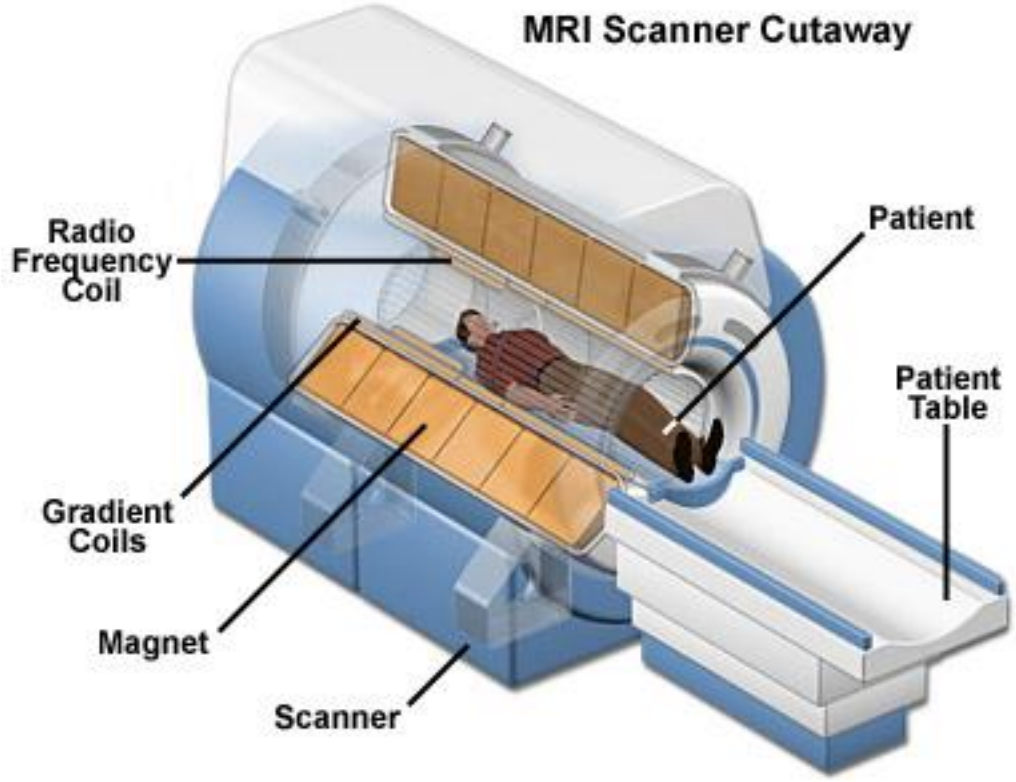

Figure 1: MRI Magnet Assembly Cutaway[1]

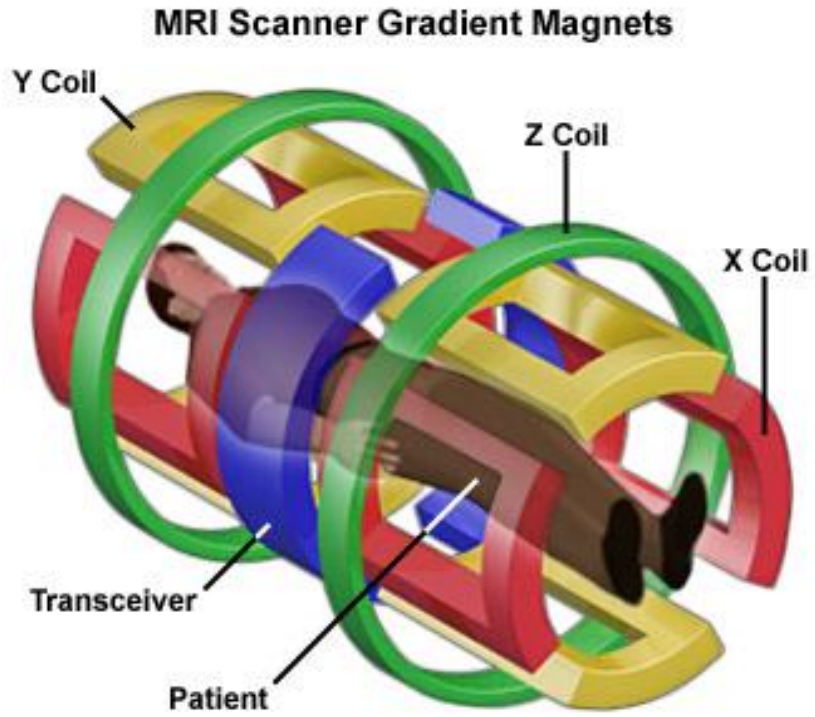

Figure 2: Magnetic Field Gradient Coils and Radiofrequency ("Transceiver") Coil within MRI Magnet Assembly[1]

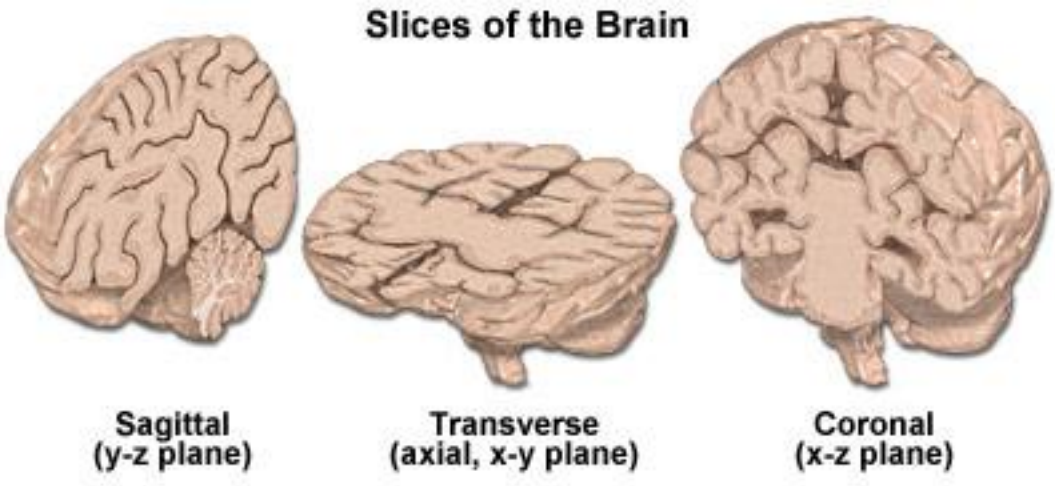

Figure 3: Nomenclature for MRI Slice Orientation in the Human Brain[1]

MRI is generally used for the imaging of soft tissues and internal organs. It is possible to differentiate the different tissues and organs on the basis of differences in their respective water concentrations, T1 and T2 relaxation times. MRIs are important noninvasive diagnostic tools; before MRIs, doctors often had to perform surgery to discover the root of a patient's problems. MRIs are

optimal in imaging because they can take images of slices of an organ or tissue and then software can put those slices together to form a three dimensional image of the tissue or organ of interest. MRI is also a preferred method of imaging because it uses non-ionizing electromagnetic radiation (radiofrequency); which means it does not break chemical bonds in the process of producing an image in contrast to x-ray imaging techniques which have the potential to do so.

ii. T_1 Weighted Images

As mentioned in the MRI background, MRI uses a very strong magnetic field to polarize hydrogen nuclei (usually from water and fat) in the body. That is, the nuclear magnetic moments of the hydrogen nuclei within the body will align themselves in either a "parallel" or "anti-parallel" orientation with respect to the direction of the main magnetic field (B_0). Statistically, about half of the nuclei align themselves in one of the two possible orientations. However, there is a slight bias for the "parallel" alignment, thus leading to a small population difference between the two orientations. The summation of the nuclear magnetic moments for the population difference results in a net magnetization vector aligned with the B_0 field direction. By convention, the B_0 field direction coincides with the +z axis of a Cartesian coordinate reference frame. The magnitude of the net magnetization vector is maximal at the Boltzmann equilibrium; i.e., the time point at which all of the nuclei have come to thermal equilibrium after placing the sample into the magnet. The magnitude of the Boltzmann equilibrium magnetization is designated as M_0. This longitudinal or z-component of the nuclear magnetization can be measured by applying a radiofrequency (RF) pulse of the appropriate frequency and magnitude.

The time decay constant at which the longitudinal or z-component of the nuclear magnetization returns to Boltzmann equilibrium is known as the T_1 relaxation time. Various tissues throughout the body have different T_1 relaxation times. By choosing optimal experimental parameters while conducting an MRI, the MR image will dramatize the effects of the T_1-relaxation-time differences between varying tissues, appearing as contrast and is denoted as a T_1 weighted image. This is a desirable effect if the T_1 of the two adjacent tissues have differing T_1 relaxation times. As will be discussed in further sections, the T_1 relaxation time difference between tissues can further be differentiated by making use of T_1 contrast agents.

Another relaxation time that may differ between tissues is the T_2 relaxation time. Images can also be weighted with T_2, as well as a third parameter, proton density. The weighting of the image is determined for each situation by adjusting the MRI experimental parameters. For T_1 weighted images, long TE and TR values are desired. The various timing parameters will be evaluated later.

iii. T_2 Weighted Images

Following the application of the RF excitation pulse, a signal-intensity decay curve can be measured as the nuclei begin to relax back to the equilibrium state. The observed time constant associated with the signal-intensity decay curve is due to the loss of phase coherence among nuclei oriented at an angle with respect to the static magnetic field. The decay time constant is denoted as T_2*. Several parameters contribute to T_2*and are summarized in the following equation:

$$\frac{1}{T_2^*} = \frac{1}{T_{2(Intrinsic\ )}} + \frac{1}{T_{2(Inhomogeneities\ )}} + \frac{1}{T_{2(Susceptibility\ )}} + \frac{1}{T_{2(Diffusion\ )}} + \cdots$$

Equation 1: Parameters which contribute T_2* decay time constant.

$T_{2(Intrinsic)}$ denotes the intrinsic spin-spin or transverse relaxation time of the nuclei themselves, $T_{2(Inhomgeneiities)}$ refers to contributions from inhomogeneities in the main magnetic field, $T_{2(Susceptibility)}$ susceptibility refers to contribution from local magnetic field inhomogeneities that arise within the tissue itself, and $T_{2(Diffusion)}$ refers to contributions from molecular water diffusion in the tissue. Thus, the value of T_2* will always be much less than or equal to the intrinsic value of T_2.

The intrinsic T_2 value of Equation 1 is one the parameters used to generate contrast in MR images by exploiting differences in this parameter for different tissues in the image. By using an MRI method based on a spin-echo RF pulse sequence, the effects of magnetic field inhomogenities and susceptibility effects (the second and third terms in the right-hand side of the above equation) can be minimized. Furthermore, diffusion effects are usually minimal when using a spin-echo pulse sequence under clinical imaging conditions. Consequently, using a spin-echo MRI pulse sequence, MR image contrast can be generated based on the intrinsic T_2 value alone. For T_2-weighted images, short TE and TR values are required; once again, these timing parameters will be discussed in later sections.

2. MRI contrast agents

In addition to the intrinsic contrast mechanisms associated with MRI (i.e., proton concentration, T1 and T2 relaxation times), various MRI contrast agents can be used to enhance the contrast (i.e., signal intensity differences) between different types of tissues being imaged. The agents are able to do this by varying the T_1 and T_2 relaxation times[1]. One class of MRI contrast agents are commonly paramagnetic metal ions such as gadolinium. The problem with the use of gadolinium and other paramagnetic metal ions alone is that they can be highly toxic. Consequently, these ions are often combined with organic

molecules to minimize their toxicity following introduction to the body. A common use for contrast agents is the diagnosis of tumors. Due to the increased permeability of tumors (particularly in the brain) relative to the surrounding normal tissue, the contrast agent can preferentially accumulate in the tumor creating strong regional contrast in the MR image.

Another class of MRI contrast agents is based on iron-oxide particles. Feridex I.V. is a super-paramagnetic iron oxide contrast agent available by AMAG Pharmaceuticals Inc. Feridex is stabilized with a dextran coating, and is administered intravenously. Feridex I.V. is currently commercially available and is widely used for the detection and diagnosis of liver lesions. According to manufacturer specifications, the concentration of iron in an I.V. dosage of Feridex is 0.56 mg Fe per Kg of body weight.

GastroMARK, also by AMAG Pharmaceuticals Inc., is also used clinically as a super-paramagnetic iron oxide contrast agent. However, this product is administered orally and is primarily used for imaging the bowel and abdominal regions.

i. T_1 and T_2 Contrast Agents

Usually, the T_2 relaxation times of cancerous tissue and surrounding normal healthy tissue have different values. For example, normal liver tissue may have a T_2 of 0.043 seconds, and a cancerous lesion found in the liver may have a T_2 of 0.056 seconds. Furthermore, cancerous tissue usually has higher T_1 values than the surrounding normal tissue. This is due to the fact that diseased tissue usually has higher water content than normal tissue, mainly due to inflammatory response. The relative differences in water content and T_1 and T_2 relaxation times between diseased and normal tissue is what gives rise to the contrast in the MR image, and allows radiologists to diagnose tumors.

ii. Iron-oxide as an MRI contrast agent

Super-paramagnetic iron oxide particles can be used as negative contrast agents. Because of their magnetic properties, they cause both inhomogenities in the local field and in the sample itself (susceptibility). The inhomogenities that the particles present lead to further decreased T_2 relaxation times of the healthy tissue. The larger difference between the two T_2 relaxation times leads to greater contrast between the healthy tissue and diseased tissue.

Iron oxide nanoparticles are particularly useful as MRI contrast agents because of their strong magnetic properties. The interaction between the water molecules in the vicinity of the strong local magnetic field of the particles results in a shortening of the T_1 and T_2 relaxation times of the water protons. The shortening of the T_2 time is due to the difference in magnetic sensitivity between the

particle medium and the surrounding tissue which causes “microscopic field gradients” that “lead to de-phasing of the proton magnetic moments”[2]. Iron oxide nanoparticles also have desirable biocompatibility and biodegradability properties; in contrast to the gadolinium MRI contrast agents discussed earlier, which can be toxic in the body.

iii. Iron Particle Concentration for MRI

To function as both a diagnostic and therapeutic agent, the concentration of iron oxide particles must be appropriate for both applications. When used as a diagnostic MRI contrast agent, Jain *et al.*[3] have shown that concentrations between 0.5 and 50 µg Fe/mL are required to effectively decrease signal intensity in an MRI. Figure 4 is from Jain *et al.* and shows the change in MRI signal intensity in a spin-echo pulse sequence as a function of the echo time (TE) for a range of concentrations of iron oxide particles. As the concentration of iron increases, the rate of signal-intensity decay also increases. Over the range of TE values typically used in clinical imaging (ranging from 10 – 90 msec), the figure shows that iron concentrations between 0.5 and 50 µg Fe/mL will provide significant signal attenuation (and hence MRI contrast) in tissue regions where the particles are sequestered (e.g., in tumors).

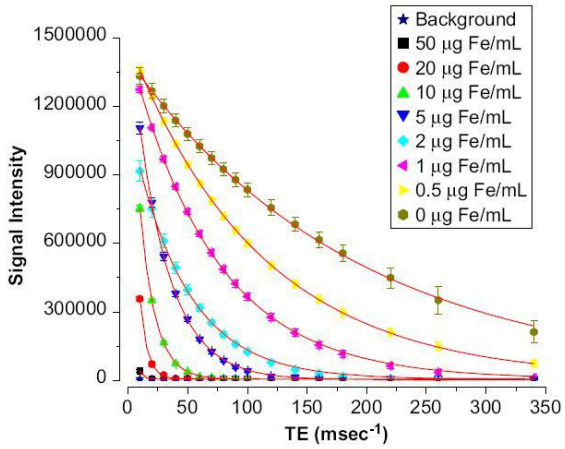

Figure 4: Plot of Signal Intensity as a Function of Echo Time (TE) for a Spin-Echo MRI Pulse Sequence for Varying Concentrations of Iron Oxide Particles.[3]

Figure 5 shows a series of MR images from solutions containing varying concentration of iron oxide particles. The signal intensity decreases steadily as the concentration of magnetic nanoparticles increases. For these MRI conditions, very effective contrast (i.e., the darker images) is achieved at concentrations between 20 and 50 µg Fe/mL. Based on the results of these studies, this iron particle concentration range is recommended for the diagnostic use of these types of agents as MRI contrast agents.

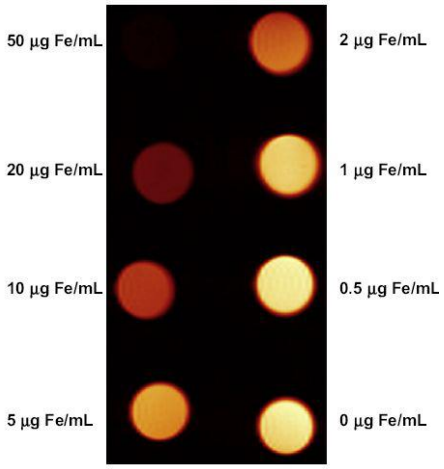

Figure 5: MR Images of Solutions with Varying Iron Oxide Concentrations[3]

3. Hyperthermia

Normal physiological temperature of the human body is about 37.0°C. Hyperthermia is the process of increasing the temperature of a particular tissue region higher than this value. Hyperthermia between 42.0°C and 46.0°C has been shown to alter the function of many structural and enzymatic proteins within cells, which leads to necrosis.[4] In addition to necrotic cell death, hyperthermia may lead to decreases in cell growth and differentiation, and can also induce apoptosis.[4] Using various targeting approaches, hyperthermia has been an effective method for treating tumors. The concept of treating tumors with hyperthermia is appealing because it is a physical treatment as opposed to a chemical one. Hyperthermia has fewer side effects than chemical treatments such as chemotherapy. Because of fewer side effects and the lack of toxicity, frequent hyperthermia treatments are possible. In chemotherapy, there is a limitation on the frequency and overall quantity of treatments because of the toxicity it imparts to the rest of the body.

Several types of hyperthermia strategies are available for tumor treatment. A highly experimental, but effective type involves magnetic embolization. Magnetic embolization hyperthermia consists of injecting magnetic particles, such as iron-oxide particles, directly to the site of treatment. When exposed to an AC magnetic field, the particles absorb energy and increase in temperature due to hysteresis loss. The rate and capacity of hysteresis loss is directly related to the specific absorption rate, or SAR. Under these conditions, magnetic particles act as heat inductors and increase the tissue temperature in the immediate vicinity of the particles. Magnetic embolization hyperthermia has been shown to be very effective because of its inherent ability for high selectivity. In one study, after five

minutes of heating, the tumor temperature reached the high forties (in degrees Centigrade) while the surrounding normal parenchyma one centimeter away from the particles remained below 40°C.[4]

i. Factors Affecting SAR: Particle Size & Surface Modifications

For effective hyperthermia treatment, a high specific absorption rate (SAR) is essential for the particles. The primary factor that affects SAR is saturation magnetization. Dennis *et. al.* for example, have shown that a difference in saturation magnetization of a factor of 1.5 yields a difference in SAR of a factor of 2.5 at 1080 Oe and 150 KHz.[5] There are several parameters of the particles that may lead to varying saturation magnetization and in turn SAR; some being particle size and surface modification.

Zhao *et. al.* have shown that particles within the size range of 10 to 30 nm are effective for hyperthermia, and found saturation magnetization to be approximately 50.05 emu/g for the given particle sample.[6] Gupta & Gupta also report saturation magnetization levels between 30 and 50 emu/g for particles that are suitable for hyperthermia treatment.[7] Dennis *et. al.* found that particles with the size of 44±13 nm and a single dextran coating have saturation magnetization around 61.64 kAm^2/g and an SAR of 537 W/gFe.[5] Additionally, they found that particles of the same core size, but with a double dextran layer, have decreased saturation magnetization at 41.08 kAm^2/g and SAR was found to be lower at 209 W/gFe.[5]

Therefore, for hyperthermia treatment, a particle size between 10 and 50 nm appears to be optimal. Because a high SAR is desired for this application, a single dextran layer should be used for a particle coating as opposed to a double layer (if dextran modifications are used). At this time, there have been no measurements of SAR for oleic-acid coated particles.

ii. Iron Particle Concentration for Hyperthermia

Differences in reporting the dosage and iron particle concentration by different investigators make it difficult to compare the results from different studies. Zhao *et. al.* suggest a concentration of 10 mg per mL of tumor volume.[6] Dennis *et. al.* have shown that doses between 722 and 976 mg of Fe are effective for hyperthermia treatment.[5] Tests were run with varying dosages, times, and magnetic field amplitudes. The total heat dose and heat dosage rate were calculated, and the maximum temperature was measured. The results of are summarized in Table 1.

Table 1: Effect of Varying Experimental Conditions on Hyperthermia Treatment in an *In Vivo* Mouse Model (from C L. Dennis *et. al.*[5]).

Group	Amplitude (Oe)	Time On (s)	Particle dose (mg of Fe)	Total heat dose ($J\ g^{-1}$ tumor)	Heat dosage rate ($J\ s^{-1}\ g^{-1}$ tumor)	Maximum temperature (°C)
1	400	900 ± 0	722 ± 50	702.50 ± 0.91	0.780	37.13 ± 1.27
2	550	1002 ± 164	845 ± 183	905.98 ± 137.37	0.904	45.27 ± 2.93
3	550	926 ± 100	436 ± 67	412.19 ± 43.05	0.445	46.80 ± 2.48
4	700	699 ± 276	976 ± 236	669.63 ± 256.51	0.958	51.16 ± 2.40
5	550	1200 ± 0	N/A	N/A	N/A	40.12 ± 2.31

For the desired final temperature of between 42.0°C and 46.0°C, Groups 2 and 3 from Table 1 meet these criteria. These groups showed that doses between 436 and 845 mg of Fe are most effective as well as exposure times between 13.67 and 19.43 minutes (Groups 3 and 2, respectively).

iii. Alternating Magnetic Field (AMF) Delivery Device

In order to induce hyperthermia using iron oxide particles, an alternating magnetic field (AMF) delivery device is employed to impart energy to the particles – resulting in a rise in temperature. Frequency, magnitude/field strength, and current of the AMF delivery device must be considered. Additionally, exposure time of the iron oxide particles to the field is a critical factor. Coil geometry must also be considered in order to accommodate varying tumor sizes and anatomical locations.

Based on the literature, the most effective range of frequencies for hyperthermia applications is between 50 and 150 KHz. One study used 80 KHz[6] and recommended AMF frequencies between 50 and 100 KHz; another study used 150 KHz[5]. Magnetic field strengths between 30 and 85 kA/m have typically been used.[5, 6]

III. Project Strategy

To optimize the application of iron-oxide nanoparticles for use as both a diagnostic and therapeutic agent, a variety of evaluations are necessary. It is of great importance to determine the initial client statement to ensure all parts of the design fit the requirements. It is also necessary to review and analyze all of the objectives based on the client statement as well as constraints. Once considering these objectives and constraints, it is necessary to review and revise the initial client statement. Finally, the actual design must be formulated and supported with a variety of analyses and background literature.

1. Client Statement and Objectives

i. Original Client Statement

Characterize the properties of Fe_3O_4 nanoparticles synthesized by Professor Yu and evaluate their potential applications as diagnostic and therapeutic agents. Following characterization of the particles, design a strategy for using iron-oxide nanoparticles in localized hyperthermia treatment of cancer cells and as MRI contrast agents.

ii. Design Objectives

To ensure an optimal design, it is necessary to consider all of the objectives required for the design. To ensure thoroughness, primary objectives were broken up into sub-categories in objectives trees. The primary objectives considered were: effectiveness, hyperthermia treatment, minimally invasive, safe, and simple-user-interface. These objectives are outlined in the following figures.

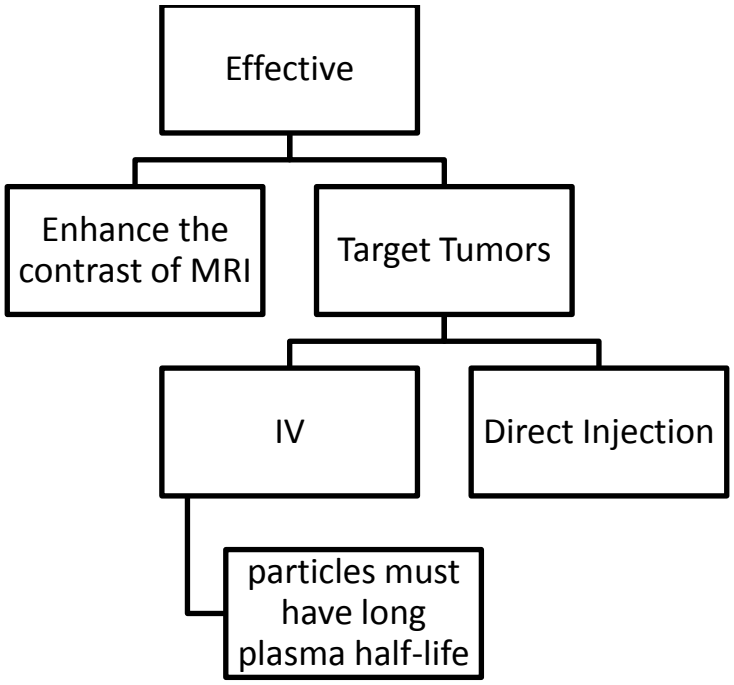

Figure 6: Objectives Tree for Effectiveness

For the design to be effective, the particles must enhance the contrast of the MRI as well as be delivered in a way that selectively targets the tumor. The effectiveness in the targeting of the tumors is considered in terms of the method of delivery. Intravenous (IV) injection requires the particles to have a long plasma half-life, so that they have the maximum opportunity to traverse the leaky vasculature that is characteristic of many tumors. Alternatively, the particles can be directly injected into the tumor. Although invasive, this method achieves a high concentration of particles at the injection site and thus improves the likelihood of success for the hyperthermia application.

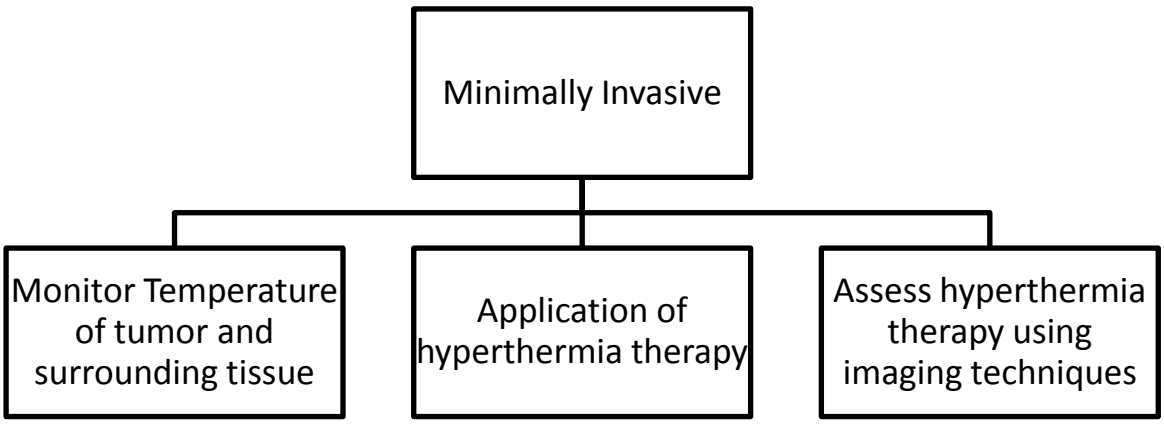

Figure 7: Objectives Tree for Minimally Invasive

It is desirable to have all aspects of the design be non-invasive to minimize potential risks – such as infection – as well as to treat tumors that are surgically inaccessible (e.g., deep within the brain). The functions that need to be performed non-invasively are: monitoring of the temperatures of the tumor and surrounding healthy tissue and application and monitoring of the therapy.

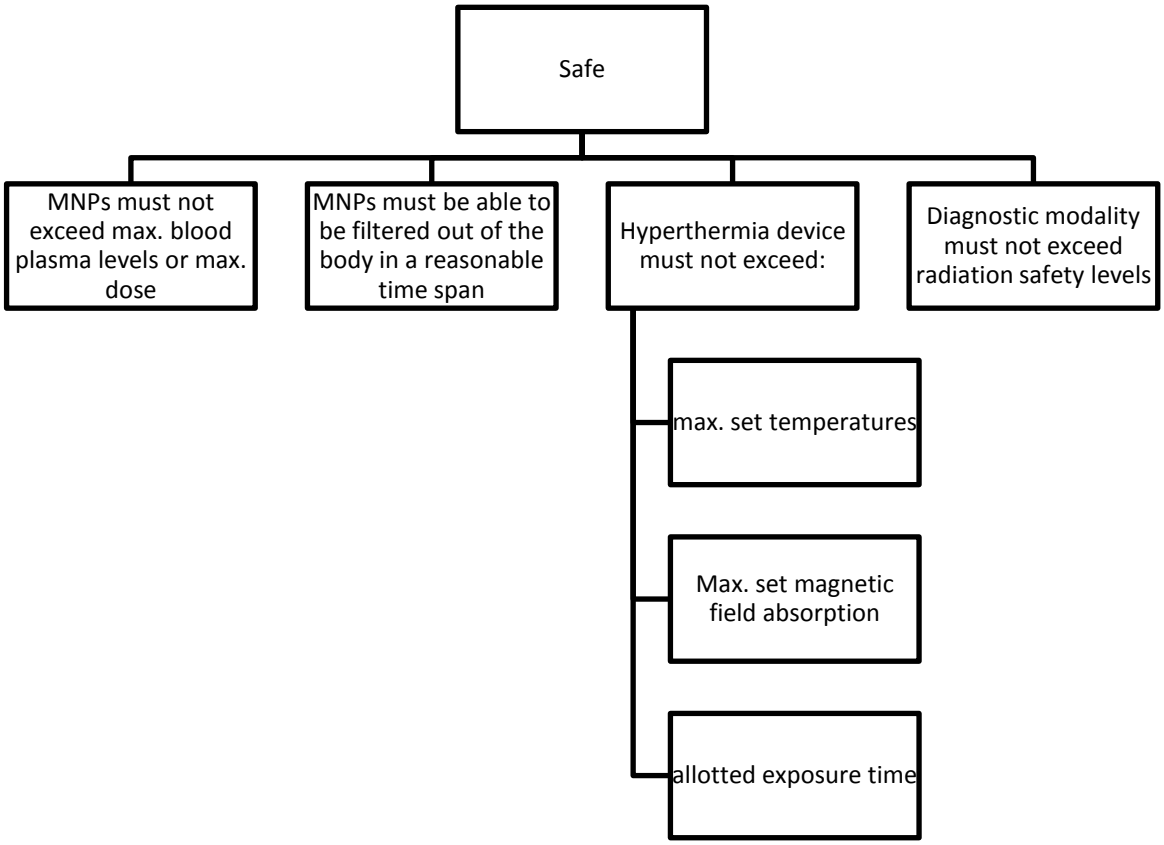

Figure 8: Objectives Tree for Safety

The objective tree for safety is of greatest importance in this design. If a design is not safe, it can never be used clinically and is thus useless. There are various categories of the design that must be considered in safety. In order to minimize toxicity, the magnetic nanoparticles (MNPs) need to be at a concentration lower than the maximum blood plasma levels or maximum dosage. They also must be bio-eliminated (cleared) from the body. Safety issues associated with the hyperthermia device include: maximum temperatures, maximum magnetic field absorption, and maximum allotted exposure time. Lastly, it is important to ensure that the diagnostic modality does not exceed radiation safety levels.

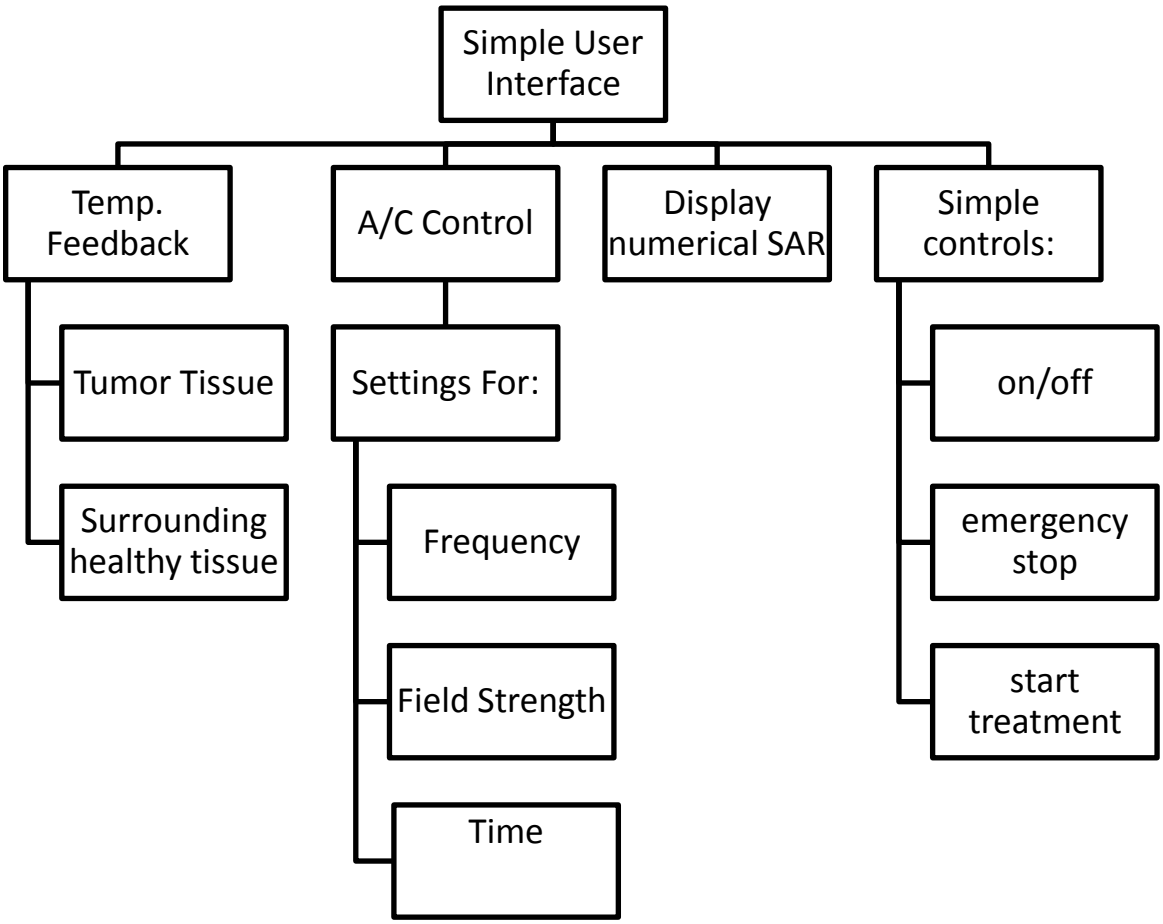

Figure 9: Objectives Tree for User Interface

To ensure effective and safe use of the product – as well as appeal to its users – the device should have a simple user interface. The user interface should be designed such that the temperature feedback for both the tumor tissue and the surrounding healthy tissue can be easily monitored for safety purposes. Another part of the interface allows control of the frequency, field strength and duration of the A/C magnetic field. It is important that these controls are simple for the user to ensure accurate therapeutic application. Additional controls are: on/off switch, an emergency stop, start treatment and a numerical display of the specific absorption rate (SAR).

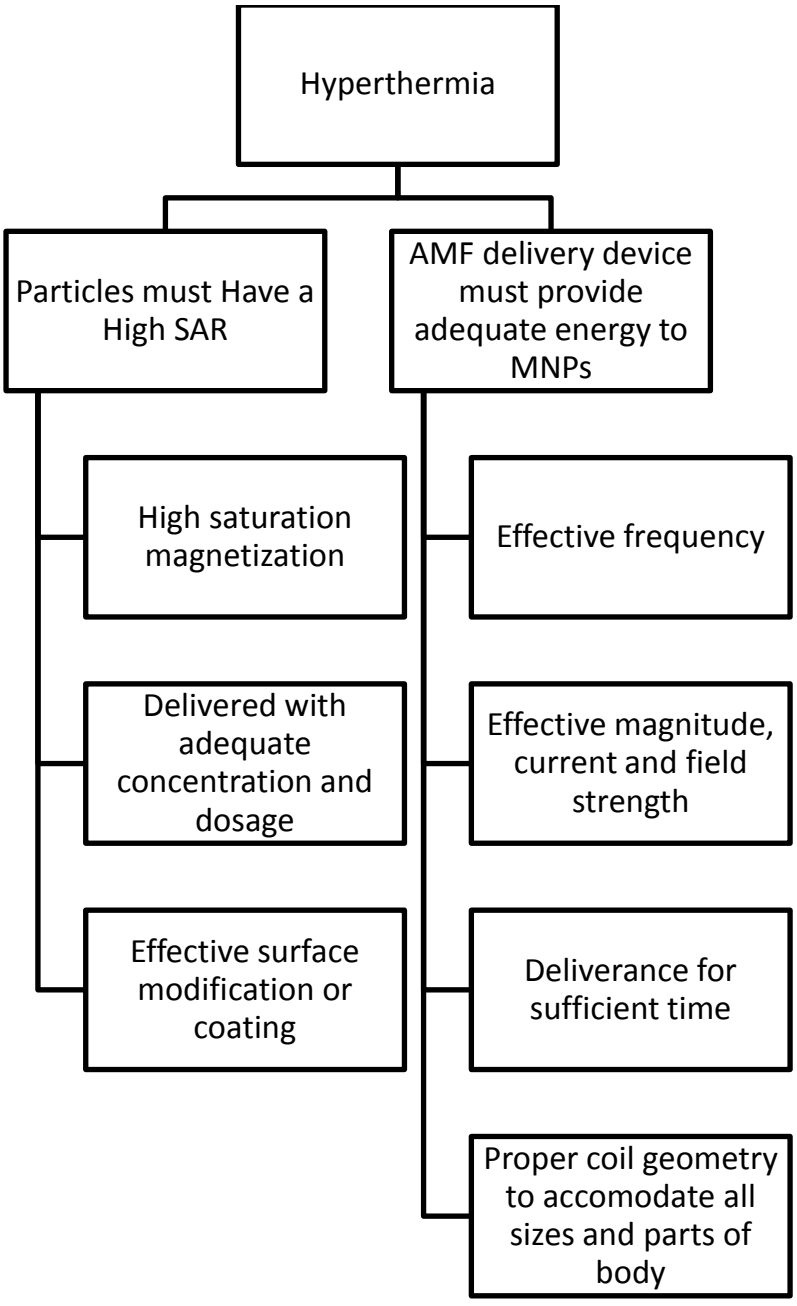

Figure 10: Objectives Tree for Hyperthermia

The objectives tree associated with hyperthermia outlines the important features of the therapeutic part of the device. There are two main branches in this objectives tree: (1) the particles must have a high SAR, and (2) the alternating magnetic field (AMF) delivery device must provide adequate energy to the magnetic nanoparticles. To have a high SAR, the particles must: (1) have high saturation magnetization, (2) be delivered with an adequate concentration or dosage, and (3) have effective surface modification or coating. For the AMF delivery device to provide adequate energy to

the MNPs, the frequency, field strength, and duration of the A/C magnetic field must be optimized. The optimization of these parameters will also be a function of the coil size and geometry; which will be determined by size and location of the anatomy that will be treated.

iii. Revised Client Statement:

After considering all of the objectives and what must be accounted for, it is necessary to revise the original client statement; the revised client statement in the following ways:

The characterization of particles is for both hyperthermia and use as a contrast agent for MR Imaging. Also, added to the client statement is that the design must be for localized hyperthermia in conjunction with MRI localization of the particles and MRI temperature monitoring of the hyperthermia treatment.

For use as an MRI contrast agent, the optimal particle size, concentration (or dose), and method of delivery must be determined. The use of iron-oxide particles as MRI contrast agents relies on their intrinsic super-paramagnetic properties. However, the strength of this effect is a function of particle size and concentration, which must be evaluated in order to produce optimal results. A frequently used approach for delivery of the particles is direct injection. However, this approach is more invasive than that of intravenous delivery, which would be the most convenient and desirable method. The toxicity and cost of the treatment must also be considered in the design. Although there are normal iron concentrations in blood, toxicity can be an issue at high concentrations.

The cost of the treatment relative to comparable current therapeutic options must also be evaluated in the design. Finally, there are a variety of potential in surface modifications to the iron oxide particles themselves that may improve the bio-distribution, delivery, and image contrast. This process would involve determining any chemical modifications of the particle surface which in turn would provide improved affinity for ligands of interest (e.g., surface proteins specific to cancer cells).

Another variable to consider in optimization of treatment is the magnitude of the AC magnetic field. The magnitude of the field must be controlled in order to obtain the most efficient level of hyperthermia while at the same time maintain a safe level of magnetic emissions. To optimize the dual functionality of the iron oxide particles, there are several variables that are common to both applications. These variables (such as particle size, dose, and method of delivery) must be optimized to best satisfy the requirements for both applications.

Based on the revised client statement, all of the needed and desired functions are considered along with possible means to accomplish these functions. The functions this design must perform along with their possible means are seen in the table below.

Table 2: Function and Means

Function	Means			
Temperature Monitoring	Measurement of T_1 relaxation time	H_2O Chemical Shift	H_2O Diffusion Measurements	IR Camera
Therapeutic Application	Focused Ultrasound	External A.C. Magnetic Field	Conventional Hyperthermia Methods	
Image Guided Therapy Assessment	MRI	CT	US	PET
Tumor Targeting	I.V. Administration	Direct Injection		

As one can see from above, all potential means of accomplishing the functions required for the design are listed. In the next chapter, a design will be formulated based on the feasibility of each of these means.

2. Alternative Designs

Every function has various means that can be used in order to achieve that function. The main objectives will be: (1) temperature monitoring of the site; (2) therapeutic application of the hyperthermia treatment; (3) the imaging technique used to monitor the status of treatment; and (4) the tumor targeting technique for the optimal delivery of the iron-oxide particles.

i. Image Guided Therapy Assessment

There are many well established biomedical imaging techniques that can be used to visualize tumors. At around $25,000-50,000[8], Ultrasound is a very inexpensive modality. It is also very safe, and easy to implement. The only safety concern is that in some instances there is undesired heating of tissue, although this is rare[9]. Ultrasound cannot penetrate bone, so imaging of the brain is impossible. It cannot penetrate gas either, so imaging of the lungs is also impossible. Thus, despite being inexpensive and easy to implement, ultrasound would be a poor choice for the imaging modality, especially if brain or lung tumors are being targeted.

CT is still relatively inexpensive, at around $160,000 for a full body scanner.[10] CT does pose a small safety risk, because the patient is exposed to X-ray radiation. Studies have shown that patients are exposed to around 22.5 mSv per full body scan[11], which is relatively low and may increase a chance of cancer of about 1 in 2000. The image quality of CT is less prone to motion artifact, and thus it is very suitable for anatomical regions which have movement such as the abdominal region.

MRI is an extremely expensive technique, at around $3,000,000 for a 3-Tesla full body scanner.[12] However, the technique is extremely safe since the patient is not exposed to high energy radiation. The only safety risk is when the patient has incompatible medical implants that may be dislodged due to the powerful magnetic field.[13] It is generally accepted that MRI has superior image quality in the brain than CT or other techniques. Because of its superior image quality, safety, and that it can be used on virtually any anatomical region, MRI is often the method of choice for tumor location and monitoring.

ii. Temperature Monitoring

In order to adhere to the client statement, the temperature monitoring modality must be non-invasive. There are several known methods which can be used in order to monitor temperature non-invasively using MRI: monitoring the T_1 relaxation time, the T_2 relaxation time, the diffusion coefficient of H_2O, or the magnetization transfer rate.

Monitoring the T_1 relaxation time is a very effective method for temperature monitoring because the measurement can be performed quickly, thus making it very suitable for hyperthermia application. A fast T_1 mapping method using TOMROP allows measurement of tissue temperature in around 4 minutes.[14] The technique is also sufficiently sensitive in that a ~1°C (shown in liver) results in a ~1-2% change in the measured value of the T1 relaxation time. [14]

T_2 relaxation time measurements have been shown to be a very ineffective method for *in vivo* temperature monitoring applications. Temperature measurements using this approach can only be made at extremely low or high temperatures, both of which are out of the physiological temperature range of interest for this project. Temperature measurements in these extreme cases would also lead to irrecoverable tissue death.[15]

Water diffusion coefficient measurements have adequate sensitivity and exhibit an ~2% change per °C; however, lengthy acquisition times make it unsuitable for hyperthermia applications. The efficacy of magnetization transfer measurements for evaluating temperature are strongly tissue dependent, and thus the general applicability of this approach to a wide range of tissue types is quite limited and not lend itself to therapeutic assessment over varying anatomical regions.

iii. Therapeutic Application

In order to achieve the project goals, hyperthermia must be employed as a therapeutic approach for treating tumors. There are three major methods of using hyperthermia for therapy. Conventional hyperthermia uses heated water jackets and relies on tissue conduction of heat to treat the affected body part. Concentrated ultrasound therapy uses ultrasound transmitters in order to heat specific tissue. Finally, the use of an alternating current magnetic field, in conjunction with magnetic nanoparticles, can exploit the hysteresis properties of the nanoparticles to heat the specified location.

A conventional hyperthermia system is displayed in Figure 11. Conventional hyperthermia is very safe because it simulates fever and improves the efficiency of the immune system for temperatures up to 40°C. However, once body temperature exceeds 42°C, studies have shown that NK-proliferation (you need to define what this is) is impaired. Conventional hyperthermia requires extremely large instrumentation (on the order of size comparable to an MRI machine). Therefore, it would be very difficult to use both MRI and conventional hyperthermia simultaneously. The heating process is also very slow; on the order of hundreds of minutes are required to achieve the desired temperature ranges.

Figure 11: BSD-2000 Conventional Hyperthermia

A current ultrasound device for use in hyperthermia has been developed by Labthermics Technologies, Inc. (LTI) and is shown in Figure 12. Concentrated ultrasound is much more specific than conventional hyperthermia because it is able to target particular anatomical regions. LTI reports that the Sonotherm 1000 can effectively and safely deliver energy as deep as 8 cm. However, ultrasound has difficulty with focusing energy selectively within irregularly-shaped tumors.

Figure 12: Sonotherm 1000 Ultrasound Hyperthermia Device

iv. Tumor Targeting

There are two major modalities of pharmacological administration that are compatible with iron-oxide nanoparticles: direct subcutaneous injection and intravenous injection.

I.V. administration can be performed by a vast majority of healthcare professionals, and will be of lower cost than a treatment requiring a physician's administration. Access can be gained by external routes, and is a low invasive modality. Additionally, it is a well-established method for drug delivery and has been proven to be very safe. Reducing the size of particles improves their stealth and maximizes the likelihood of reaching targeted tissues. Particles larger than 200 nm are very efficiently cleared from the vasculature by phagocytotic cells of the spleen, while particles smaller than 5.5 nm are removed through renal clearance.[16] As long as particles are between 5.5 nm and 200 nm in size, I.V. administration may prove to be a very effective method by maximizing the residence time in the vasculature which in turn increases the likelihood of tumor uptake of the particles .

Direct injection may require surgery and a skilled physician in order to effectively administer the particles. This does not adhere to the non-invasive requirement of the client statement. The safety of direct injection is also compromised if a tumor site such as the brain is being targeted. However, direct injection does guarantee the highest percentage of particle delivery to a given area.

v. Pairwise Comparison Charts

The following functions have potential to be fulfilled with varying means: temperature monitoring, therapeutic application, tumor targeting, and image guided therapy assessment. First, the various attributes of each function were weighed against each other. The proceeding tables summarize this weighting process. When the function on the left column is more important than the function on the top row, a "1" is placed in the cell; otherwise a "0" is placed in the cell. A final score is computed by summing the row for each function. The weight is then determined by dividing the individual score for each function by the total score of all functions. Some of the totals of weight are 110% in order to avoid ease of use being negated completely.

Table 3: Temperature Monitoring

	Cost	Compatibility with AMF Device	Safety	Easy To Use	Sensitivity	Reading Time	**Score**	**Weight**
Cost		0	0	1	0	1	2	0.13
Compatibility with AMF Device	1		0	1	0.5	1	3.5	0.23
Safety	1	1		1	1	1	5	0.33
Easy To Use	0	0	0		0	0.1	0.1	0.01
Sensitivity	1	0.5	0	1		1	3.5	0.23
Reading Time	0	0	0	1	0		1	0.07
						Totals=	15.1	110%

Table 4: Therapeutic Application

	Cost	Compatibility with Imaging	Safety	Easy To Use	Energy Delivery	**Score**	**Weight**
Cost		0	0	1	0	1	0.10
Compatibility with Imaging	1		0.5	1	1	3.5	0.35
Safety	1	0.5		1	0.5	3	0.30
Easy To Use	0	0	0		0	0.1	0.01
Energy Delivery	1	0	0.5	1		2.5	0.25
					Totals=	10.1	100%

Table 5: Image Guided Therapy Assessment

	Cost	Interference to AMF Device	Interference from AMF Device	Easy To Use	Image Quality	Safety	**Score**	**Weight**
Cost		0	0	1	1	0	2	0.13
Interference to AMF Device	1		0.5	1	1	0	3.5	0.23
Interference from AMF Device	1	0.5		1	1	0	3.5	0.23
Easy To Use	0	0	0		0.5	0	0.5	0.03
Image Quality	0	0	0	0.5		0	0.5	0.03
Safety	1	1	1	1	1		5	0.33
						Totals=	15	110%

Table 6: Tumor Targeting

	Cost	Non-Invasiveness	Safety	Easy To Use	Particle Delivery	**Score**	**Weight**
Cost		0	0	1	0	1	0.10
Non-Invasiveness	1		0	1	0	2	0.20
Safety	1	1		1	0.5	3.5	0.35
Easy To Use	0	0	0		0	0.1	0.01
Particle Delivery	1	1	0.5	1		3.5	0.35
					Totals=	10.1	110%

vi. Numerical Evaluation Matrices

Once the attributes are weighted, the different means can be scored against each other. The means are ranked from one to the number of means for that function. For example, therapeutic application has three means, so for each attribute (cost, safety, etc), the means are ranked from one to three; where three is the best in that category and one is the worst. The weighting from the previous section determines how much that attribute will contribute to the final score of that mean as a total. Lastly, the final score will determine what means will be chosen for the design (higher score is better). The final decisions are selected in red.

Table 7: Temperature Monitoring

	Sensitivity	Reading Time	**Score**
Proton Density	5*0.23=1.15	5*0.07=0.35	1.50
T1 Relaxation Time	6*0.23=1.39	6*0.07=0.42	1.81
T2 Relaxation Time	1*0.23=0.23	1*0.07=0.07	0.30
Diffusion	4*0.23=0.92	1*0.07=0.07	0.99
Magnetization Transfer	1*0.23=0.23	1*0.07=0.07	0.30
Proton Resonance Frequency (PRF)	1*0.23=0.23	1*0.07=0.07	0.30

Table 8: Therapeutic Application

	Cost	Compatibility with Imaging	Safety	Easy To Use	Energy Delivery	**Score**
Focused Ultrasound	3*0.10=0.30	2*0.35=0.70	2*0.30=0.60	1*0.01=0.01	2*0.25=0.50	2.11
External A.C. Magnetic Field	2*0.10=0.20	3*0.35=1.05	3*0.30=0.90	1*0.01=0.01	3*0.25=0.75	2.91
Conventional Hyperthermia Means	1*0.10=0.10	1*0.35=0.35	1*0.30=0.30	3*0.01=0.03	1*0.25=0.25	1.03

Table 9: Image Guided Therapy Assessment

	Cost	Interference to AMF Device	Interference from AMF Device	Easy To Use	Image Quality	Safety	**Score**
MRI	1*0.13=0.13	1*0.23=0.23	3*0.23=0.69	1*0.03=0.03	3*0.03=0.09	2*0.33=0.66	1.83
CT	2*0.13=0.26	2*0.23=0.46	2*0.23=0.46	2*0.03=0.06	2*0.03=0.06	1*0.33=0.33	1.63
US	3*0.13=0.39	3*0.23=0.69	1*0.23=0.23	3*0.03=0.09	1*0.03=0.03	1*0.33=0.33	1.76

Table 10: Tumor Targeting

	Cost	Minimal-Invasiveness	Safety	Easy To Use	Particle Delivery	**Score**
I.V. Administration	2*0.10=0.20	2*0.20=0.40	2*0.35=0.70	2*0.01=0.02	1*0.35=0.35	1.67
Direct Injection	1*0.10=0.10	1*0.20=0.20	1*0.35=0.35	1*0.01=0.01	2*0.35=0.70	1.36

3. Conceptual Design

After thorough analysis and consideration of all objectives, functions, means and constraints, the optimal design for iron-oxide nanoparticles as a hyperthermia agent is formulated as follows. Iron oxide nanoparticles will be intravenously injected into the blood stream. Due to leaky vasculature, the particles will concentrate in the tumor while any excess particles in other locations are cleared from the body. An MRI can be used to confirm the localization of the particles in the tumor. Once this confirmation is complete, an AMF device delivers an A/C magnetic field to the tumor, heating the particles. As the particles are heated, MRI temperature monitoring is done to ensure normal physiological temperatures of the healthy surrounding tissue, and to monitor the temperature of the tumor. As the particles are heated, the cancerous tumor cells are minimized. MRI is used to monitor the ablation of the tumor along with the temperature. After treatment is completed, the body will filter out the particles. This conceptual design can be seen in the illustration below (Figure 13: Illustration of conceptual design for hyperthermia treatment and particle delivery

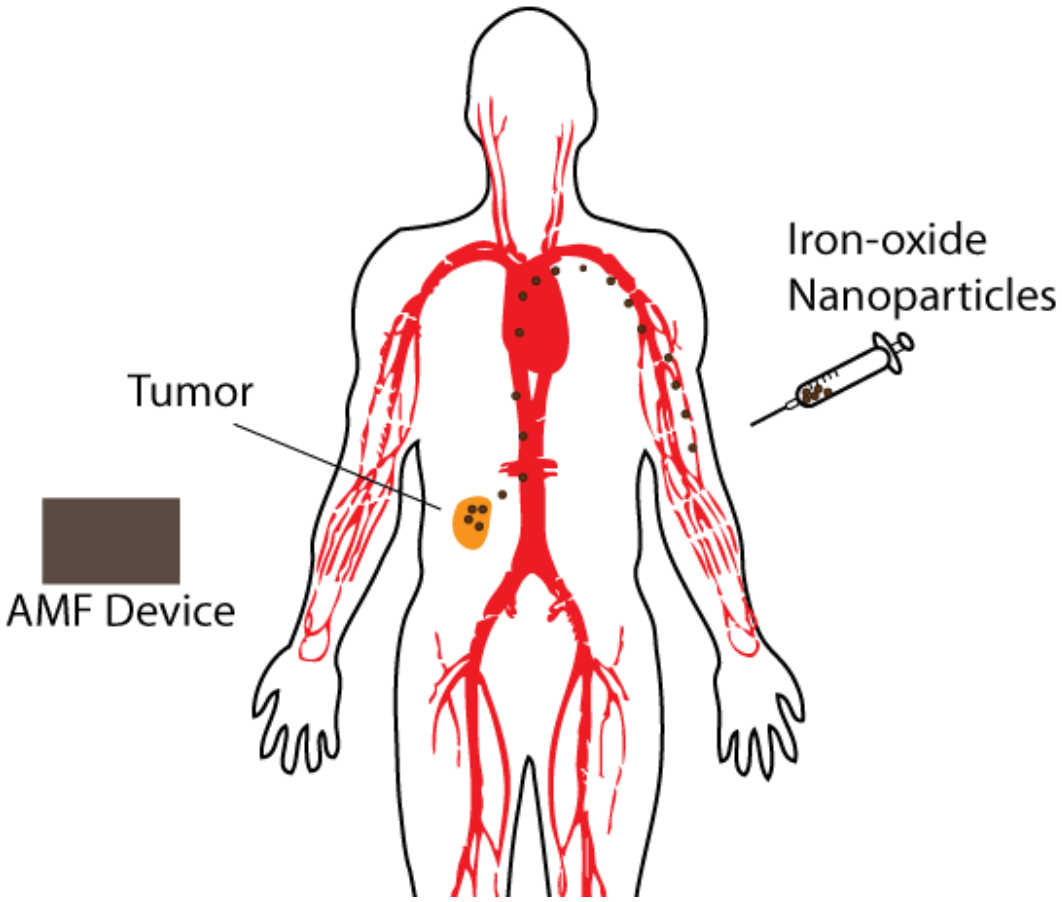

Figure 13: Illustration of conceptual design for hyperthermia treatment and particle delivery

IV. Experimentation

1. Inversion Recovery Background

Method to measure T_1

Inversion recovery (IR) is a nuclear magnetic resonance (NMR) technique used to measure the T1 (spin-lattice) relaxation time of nuclear spins. In this method, the net magnetization vector, M_0, is inverted (i.e., rotated from the +z axis to the –z axis of the Cartesian coordinate reference frame) using a 180° RF pulse (see Fig. 1). During the time period TI following the 180° RF pulse, the nuclei will relax back to their Boltzmann equilibrium alignment by dissipating energy to their surroundings (i.e., the "lattice"). Before the magnetization fully returns to the Boltzmann equilibrium, however, a 90° RF pulse is applied in order to flip the magnetization into the transverse plane. Once in the transverse plane, the magnetization vector length can be measured (because longitudinal magnetization cannot be measured directly). At shorter values of TI, the magnitude of the longitudinal magnetization vector will be negative. At longer values of TI, the longitudinal magnetization vector becomes positive. The longitudinal magnetization recovers exponentially back to the Boltzmann equilibrium with a time constant that is equal to T_1.

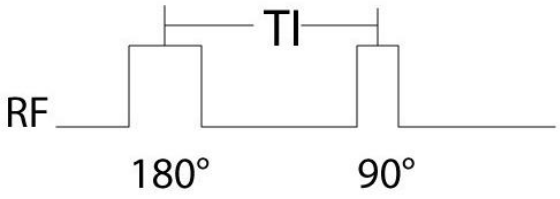

Figure 14: Inversion Recovery RF Pulse Sequence

The Bloch equation for inversion is shown below, where $M_z(t)$ is the acquired magnetization at time t (or TI in Figure 14), M_0 is the Boltzmann equilibrium magnetization, and T_1 is the relaxation time of the nuclei being measured.

$$M_z(t) = M_0\left(1 - 2e^{-t/T_1}\right)$$

Equation 2

It is clear that with sufficient data samples, $M_z(t)$, at varying times, the T_1 of the material can be calculated. As previously mentioned, the measurements of M_z are closest to $-M_0$ at earlier acquisition times, and closest to M_0 at the later acquisition times.

2. NMR T_1 Relaxivity Measurements

Inversion recovery was used to measure the T_1 relaxation time for the iron-oxide particles. The signal intensity is measured at intervals of TI, for a total of 23 measurements for each concentration. The first measurement was taken at TI = 0.005s, and the last measurement was taken at TI= 8s. Figure 15 shows inversion recovery plots for the 14.4 nm particles as a function of concentration. Figure 16 shows the analogous plots for the 32.4 nm particles.

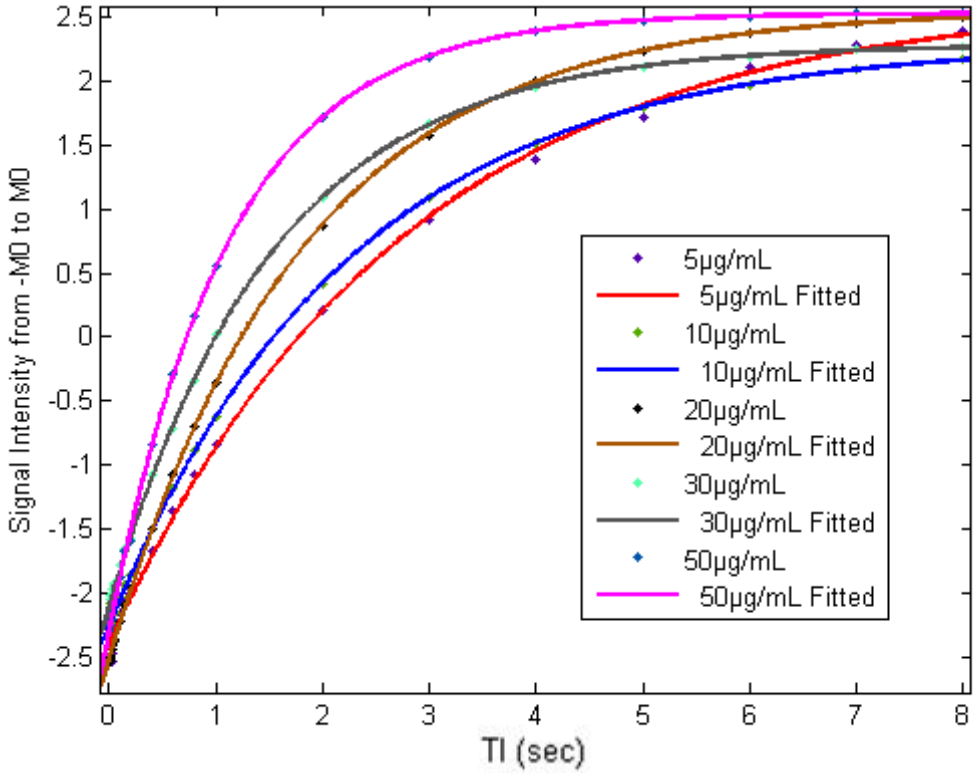

Figure 15: Plot Inversion recovery data for 14.4 nm iron-oxide particles as a function of concentration.

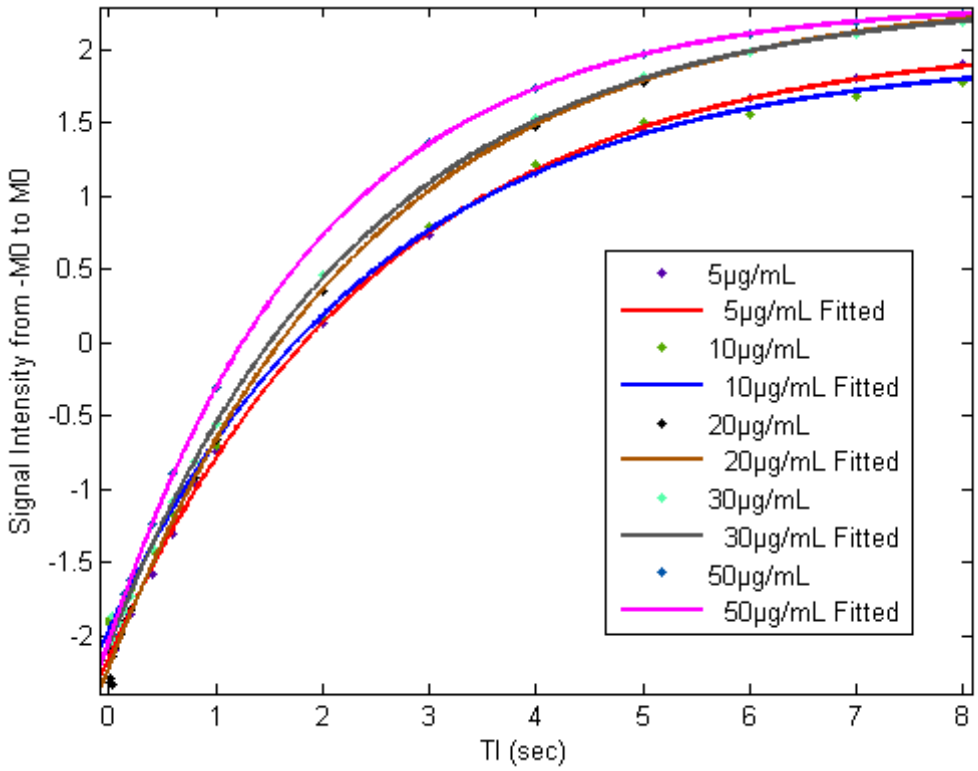

Figure 16: Plot of Inversion recovery data for 32.4 nm iron particles as a function of concentration.

The relaxation curves shown in the above plots were fitted to Equation 1 using MATLAB's Curve Fitting Toolbox and the T_1 relaxation time was calculated at each concentration. The relaxation rates, R_1 (=1/T_1), were then calculated at each concentration and these data are summarized in the following table.

Table 11: R_1 (1/sec) and T_1 (sec) for 14.4nm and 32.4nm iron particles as a function of concentration

Concentration (µg/mL)	T1, 14.4nm	R1, 14.4nm	T1, 32.4nm	R1, 32.4nm
5	2.76	0.36	2.59	0.39
10	2.27	0.44	2.53	0.40
20	1.81	0.55	2.44	0.41
30	1.53	0.65	2.40	0.42
50	1.12	0.89	2.00	0.50

The R_1 values were then plotted as a function of concentration and linear regression was performed on the data to determine the slope of the best-fit straight lines. The slope of the line is referred to as the relaxivity, r_1, and is a measure of the efficiency with which the particles promote spin-lattice (T_1) relaxation. The squared correlation coefficient, R^2, 0.997 for the 14.4nm particles and 0.903

for the 32.4nm particles, demonstrated a good linear correlation of the data. The r_1 value for the 14.4 nm particles is 11.5 x 10^{-3} mL(sec^{-1})(μg^{-1}). The 32.4 nm particles have an r_1 value of 2.4 x 10^{-3} mL(sec^{-1})(μg^{-1}).

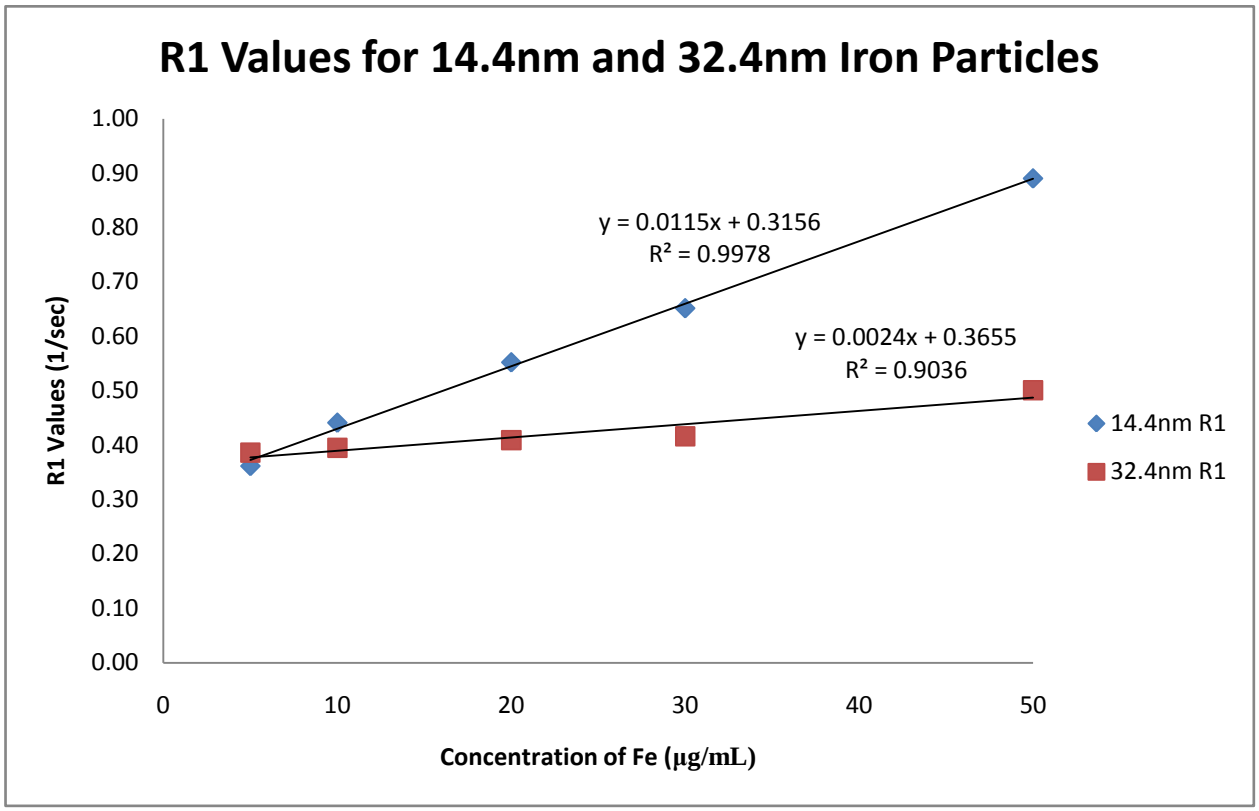

Figure 17: Plot of R1 relaxation rates for 14.4nm and 32.4nm iron particles as a function of concentration. The slope of each line corresponds to the relaxivity, r_1, for each particle size.

3. Hahn Spin Echo Background

Method to measure T_2

The Hahn spin echo (SE) method is used to measure the T_2 (transverse) relaxation time of nuclear spins. The SE begins with a 90° radio frequency (RF) excitation pulse (see Figure 18), which rotates the longitudinal magnetization into the transverse plane. The transverse magnetization then begins to precess about the longitudinal axis. During this process, the precessional speed of the individual nuclear magnetic moments that comprise the transverse magnetization will vary slightly; resulting in a de-phasing (and hence attenuation) of the magnetization vector. After a waiting period *t*, a 180° RF pulse is applied in order to reverse the positional relationship between individual nuclear magnetic moments in the transverse plane. In this case, the faster precessing nuclei will now be

positioned *behind* the slower precessing nuclei (as compared to being *ahead* prior to the application of the 180° RF pulse). After a second time *t* has elapsed, the transverse magnetization will re-phase and is attenuated only by the intrinsic T_2. The 180° RF pulse effectively rids the T_2 measurement of any dependence on B_0 field inhomogeneities or susceptibility effects arising from the sample. The equation which describes the SE signal intensity is shown below:

$$M_z(2t) = M_0\left(e^{-2t/T_2}\right)$$

Equation 3

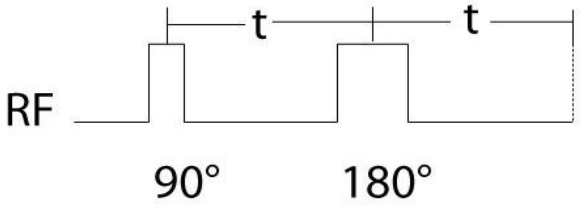

Figure 18: Hahn Spin Echo RF pulse sequence

4. NMR T_2 Relaxivity Measurements

The Hahn spin echo was used to perform the T_2 relaxation analysis on the iron-oxide particles as a function of concentration (5, 10, 20, 30, and 50µg/mL). The SE signal intensities were acquired for increasing echo times (TE; where TE = 2t in Equation 3). The T_2 relaxation analysis was performed for both 14.4 nm and 32.4 nm particles. The measurement results are shown in Figure 19 and Figure 20.

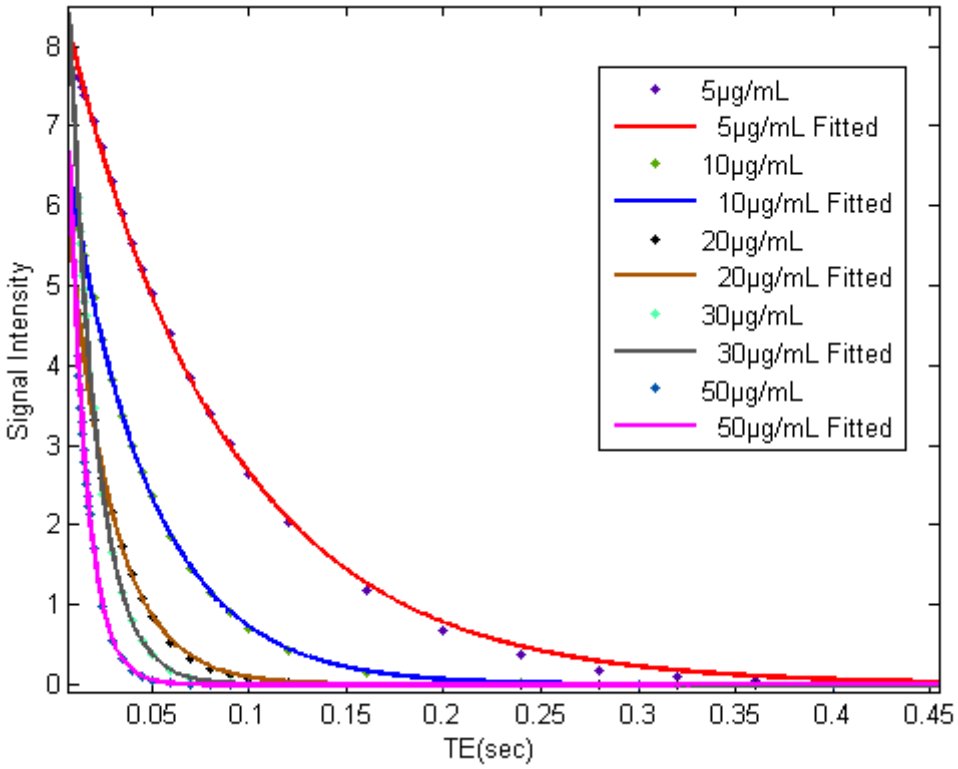

Figure 19: Plot of spin echo signal intensity as a function of echo time (TE) for 14.4nm iron oxide particles at various concentrations.

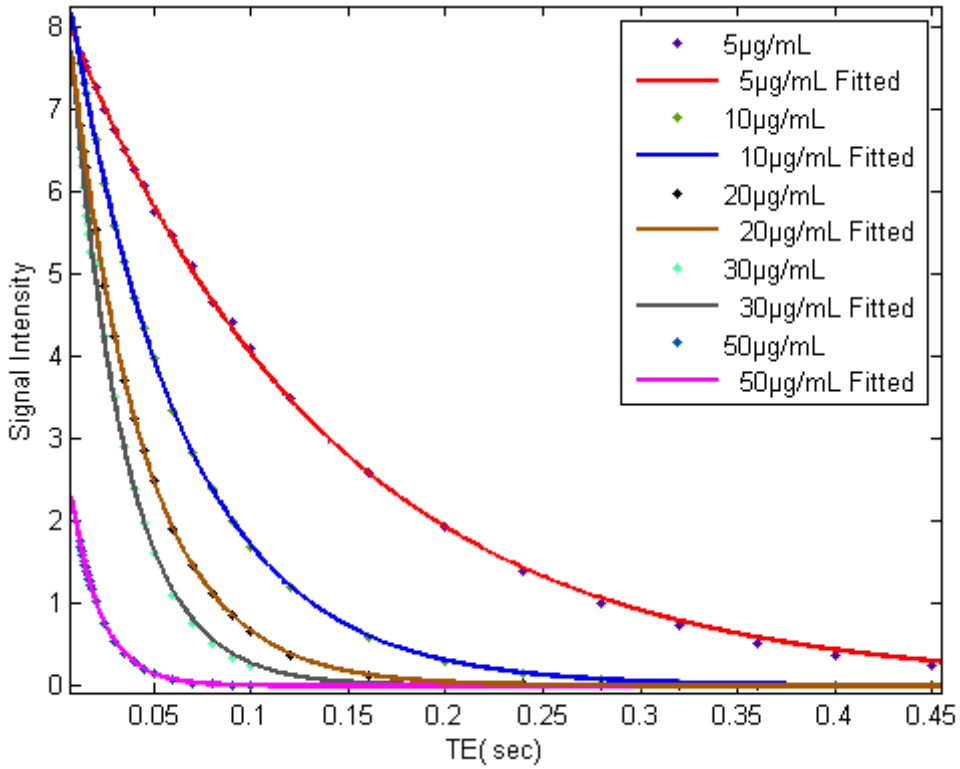

Figure 20: Plot of spin echo signal intensity as a function of echo time (TE) for 32.4nm iron oxide particles at various concentrations.

This relaxivity data was fitted using the following exponential formula in Equation 3, the corresponding fitted data is shown in Figure 19 and Figure 20 using MATLAB's Curve Fitting Toolbox and the T_2 relaxation time was calculated at each concentration. The relaxation rates, R_2 (=1/T_2), were then calculated at each concentration and these data are summarized in the following table.

Table 12: R_2 (1/sec) and T_2 (sec) for 14.4nm and 32.4nm iron particles as a function of concentration.

Concentration (µg/mL)	T2, 14.4nm	R2, 14.4nm	T2, 32.4nm	R2, 32.4nm
5	0.0820	12.19	0.1353	7.39
10	0.0424	23.57	0.0588	17.01
20	0.0227	44.09	0.0377	26.50
30	0.0137	72.94	0.0276	36.21
50	0.0091	110.27	0.0155	64.52

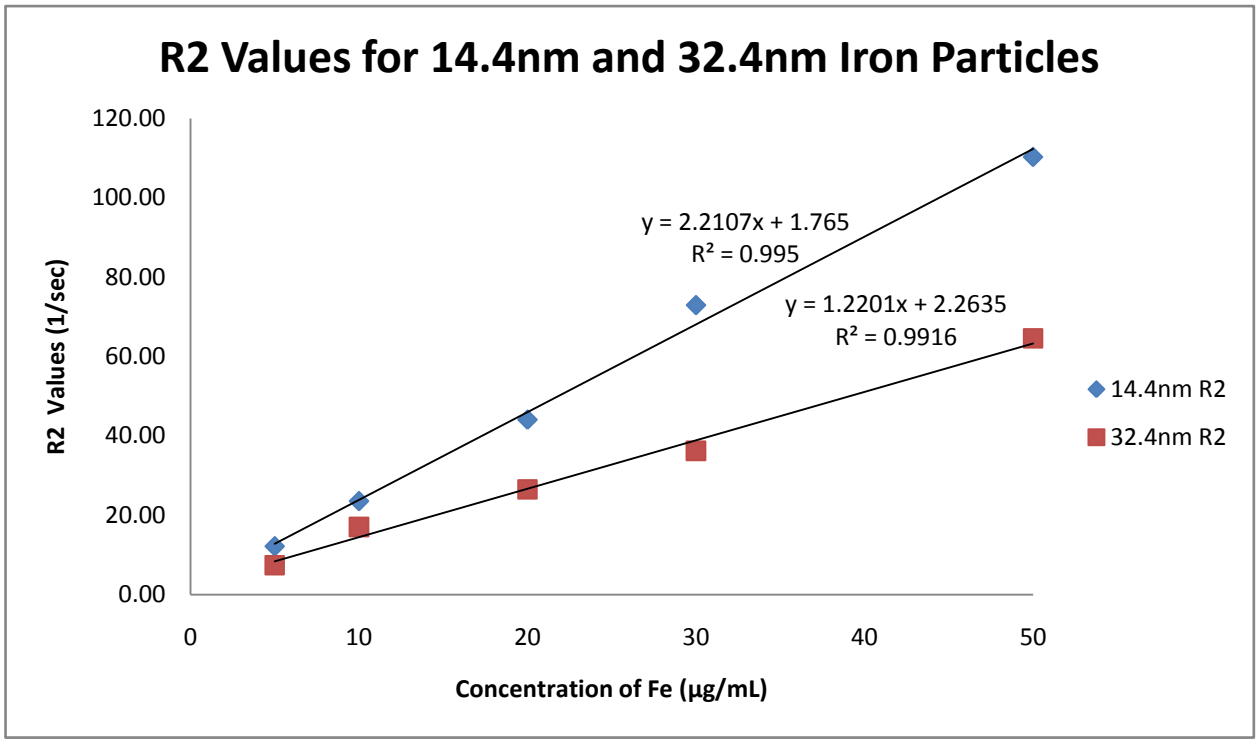

Figure 21: r_2 values for 14.4nm and 32.4nm

The R_2 values were then plotted as a function of concentration and linear regression was performed on the data to determine the slope of the best-fit straight lines. The slope of the line is referred to as the relaxivity, r_2, and is a measure of the efficiency with which the particles promote spin-spin (T_2) relaxation. The squared correlation coefficient, R^2, 0.995 for the 14.4nm particles and 0.991 for the 32.4nm particles, demonstrated a good linear correlation of the data. The r_1 value for the 14.4 nm particles is 2.21 mL(sec^{-1})(μg^{-1}). The 32.4 nm particles have an r_1 value of 1.22 mL(sec^{-1})(μg^{-1}).

5. Summarized Relaxivity Results

Table 13: T1 and T2 relaxivities of the 14.4nm and 32.4nm Iron-oxide particles

Sample	T_1 Relaxivity (r_1) $mL(sec^{-1})(\mu g^{-1})$	Squared Correlation Coefficient (R^2)	T_2 Relaxivity (r_2) $mL(sec^{-1})(\mu g^{-1})$	Squared Correlation Coefficient (R^2)
14.4nm Iron Particle	11.5×10^{-3}	0.9978	2.21	0.995
32.4nm Iron Particle	2.4×10^{-3}	0.9036	1.22	0.9916

6. Experimental Analysis

Iron-oxide nanoparticles are excellent candidates for brain tumor contrast enhancement. Normal brain tissue is protected by the blood-brain barrier; however, tumors possess leaky vasculature and have often compromised the blood-brain barrier. The lack of a blood-brain barrier in the vicinity of brain tumors gives rise to an excellent opportunity for the tumor to uptake particles for therapeutic or diagnostic applications. In order to effectively use the iron-oxide nanoparticles as an MRI contrast agent, they must be characterized using nuclear magnetic resonance.

Brain tissue is divided into two major classifications: white and gray matter. The central portion of the brain consists of white matter which contains the interconnections of the brain structures. The outer coating of the brain consists of gray matter. A previous study showed that the average T_1 value for gray and white matter was 1331 and 832 msec, respectively, at 3.0 Tesla.[17] Average T_2 values for gray and whiter matter are 80 and 110 msec, respectively, at 3.0 Tesla.[17] Higher relaxation times are present in gray matter due to the higher water content. Even higher relaxation times are expected in tumors. Based on 1.5 and 8.5 Tesla measurements, the relaxation times for a tumor can be estimated to be typically around 1500 msec and 135 msec for T_1 and T_2, respectively. While it has been found that the water content of the brain overall is around 77%, studies have shown that the white matter is approximately 70% water[18], and the gray matter is approximately 80% water[19]. The water content of gray matter is very close to that of the water content in tumor tissue. The water content in tumor tissue is usually around 83%[20], however, it can vary greatly. The water content of a tumor is the highest for any tissue of interest. For this reason, for the analysis, proton density will be normalized to that for the tumor. The proton density for white and gray matter can be relatively adjusted and are shown in the following table, along with other parameters of interest.

Table 14: Average relaxation times, water content, and relative proton density for white and gray matter, and a typical tumor

	T_1 (msec)	**T_2 (msec)**	**Water Content**	**Proton Density**
White Matter	832	80	70%	0.84
Gray Matter	1331	110	80%	0.96
Tumor	1500 (Estimate)	135 (Estimate)	83%	1.0

As shown in the previous section, the following equations can be used to characterize the R_1 and R_2 (relaxation rates) for the different particle sizes at 3.0 Tesla:

$$R_1(14.4\,nm) = 0.011 * Conc + 0.315$$
$$R_1(32.4\,nm) = 0.002 * Conc + 0.365$$
$$R_2(14.4\,nm) = 2.210 * Conc + 1.765$$
$$R_2(32.4\,nm) = 1.220 * Conc + 2.263$$

Equation 4: Relaxation rates at 3T for iron-oxide particles in solution

However, these NMR results were observed while the particles were in solution. Since the particles will be used for contrast enhancement in tumors, the y-intercept of the previous equations can be replaced with the R_1 and R_2 values for a typical tumor. Previously, it has been estimated that tumor T_1 and T_2 are approximately 1500 and 135 msec, respectively. $R_{1,2}$ values are simply the inverse of $T_{1,2}$ values, so the typical R_1 and R_2 of a tumor are around 0.67 and 7.4 $msec^{-1}$, respectively. The collective equations for the relaxation rates for a tumor with the particles infused are shown in the following equations:

$$R_1(14.4\,nm) = 0.011 * Conc + 0.67$$
$$R_1(32.4\,nm) = 0.002 * Conc + 0.67$$
$$R_2(14.4\,nm) = 2.210 * Conc + 7.4$$
$$R_2(32.4\,nm) = 1.220 * Conc + 7.4$$

Equation 5: Relaxation rates at 3T for tumors with embedded particles

…where *Conc* is the concentration of iron in μg/mL and the R values will be given in $msec^{-1}$.

The results of the previous equations are shown in the following plots creating in MATLAB:

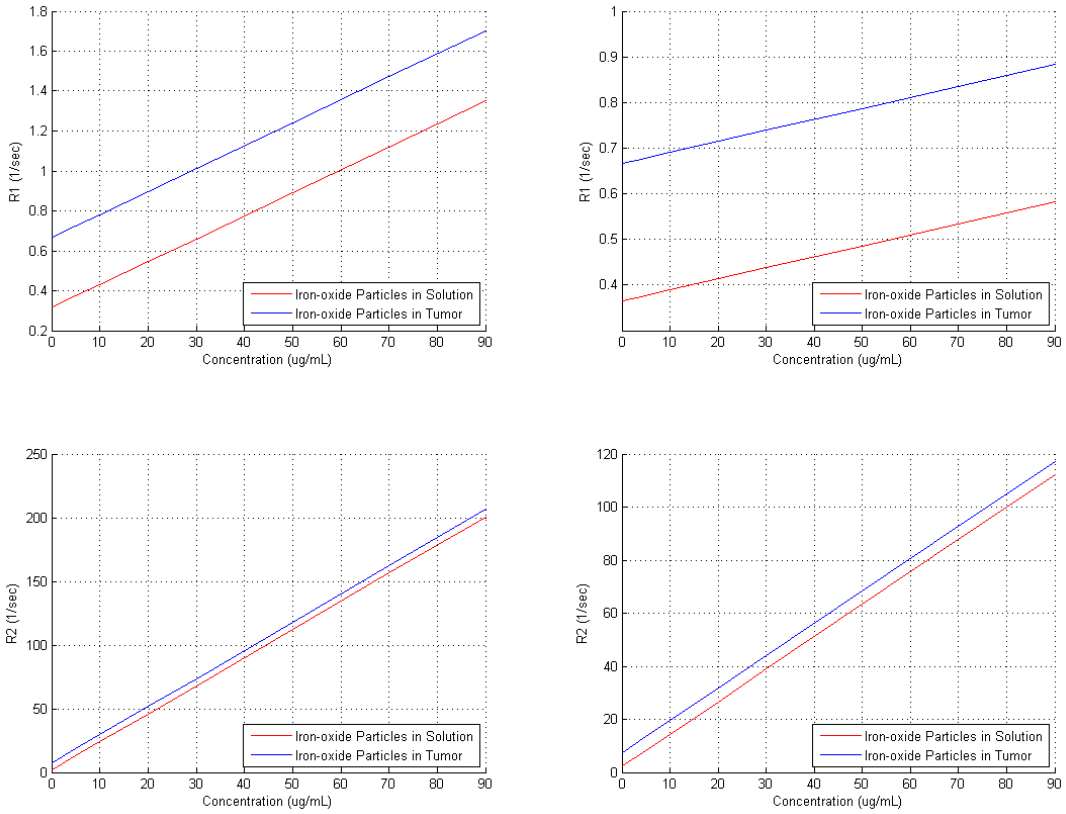

Figure 22: Water relaxation rates for iron-oxide particles in solution and in tumor as a function of concentration: R_1 of 14.4nm (top left), R_1 of 32.4nm (top right), R_2 of 14.4nm (bottom left), and R_2 of 32.4nm (bottom right).

Using Equation 5 or Figure 22, the relaxation rates can be determined, either mathematically or graphically, for the tumor with embedded particles for any concentration of iron. The relaxation rates of the tumor with embedded particles can then be used in order to determine the effects of concentration on signal intensity. First, T_1 relaxation analysis will be performed for effects of signal intensity on T_1-weighted image contrast.

The average T_1 relaxation times were used in order to construct T_1 relaxation curves for normal white and gray matter. A T_1 relaxation curve for a typical tumor was also plotted, based on the estimated relaxation time. Lastly, a series of curves were plotted which use the data from the relaxation rate equations for tumors with varying concentrations of particles. The relaxation curves were modeled using the following equation:

$$M_z(TR) = M_0(1 - e^{-TR/T_1})$$

Equation 6

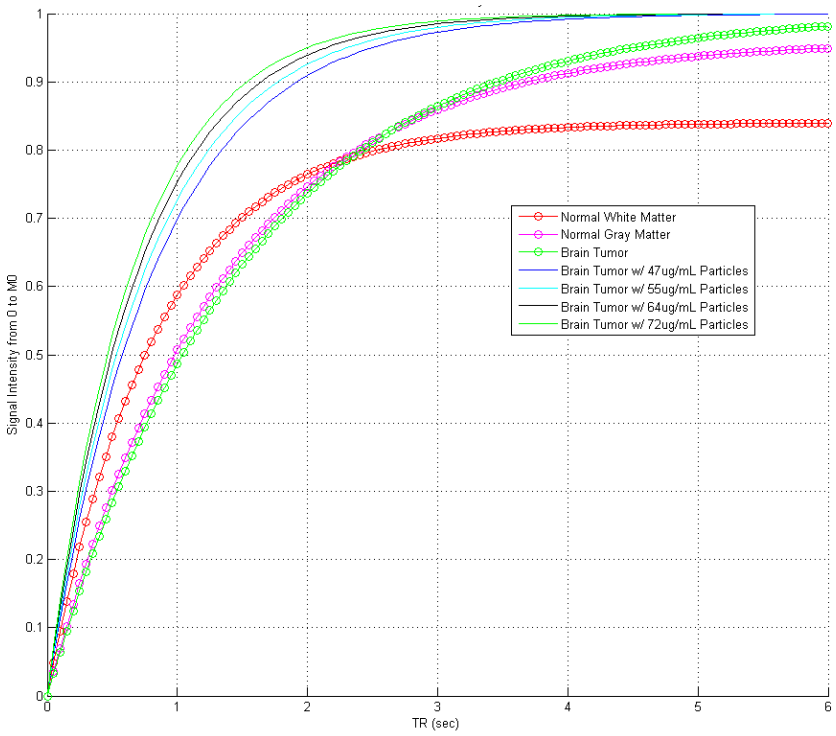

Figure 23: T_1 relaxation analysis for normal white and gray matter, a typical brain tumor, and brain tumor with 14.4nm particles of varying concentrations.

In Figure 23, normal white matter is shown relaxing to a normalized Boltzmann equilibrium value of around $0.84M_0$; due to its relative low water content compared to gray matter and brain tumors as shown in Table 14. Gray matter relaxes to a Boltzmann equilibrium signal intensity of around $0.96M_0$ and the brain tumor relaxes to the normalized value of M_0. For a T_1-weighted image, short TE and short TR values are typically used. If a typical TR value is chosen, for example 500 msec, the signal intensities between the different tissue types can be measured at that time. Shown in Figure 23 are the T_1 curves of the tumor with particles at varying concentrations. The particles used in the above plot are 14.4nm due to the relaxation benefits that they provide as determined and shown in the linear relaxation rate plots. In order to give rise to signal intensity differences (and thus give rise to contrast), an R_1 relaxation rate of around 1.2 sec^{-1} is necessary, which particles at around 47 µg/mL provide when embedded in a tumor. 47 µg/mL is the lowest usable concentration of particles to provide contrast. Also shown in the plot above are the relaxation curves for tumors with 55 µg/mL, 64 µg/mL and 72 µg/mL.

Using a percent difference equation, the signal intensity difference between normal tissue and tumors with particles can be calculated. For example:

$$\%\ Difference = \frac{SI_{TP} - SI_N}{SI_N} * 100$$

Equation 7: Percentage of difference calculation for signal intensities

where SI_{TP} is the signal intensity of the tumor with particles, and SI_N is the signal intensity of the normal surrounding tissue. This example can be applied for a tumor with particles of concentration of 72 µg/mL and surrounding white matter at a TR of 500 msec:

$$\%\ Difference = \frac{0.53 - 0.38}{0.38} * 100 = 39\%$$

Equation 8: Percentage of signal intensity difference between normal white matter and a tumor with a concentration of 14.4nm particles of 72 µg/mL

When using iron-oxide particles of 14.4nm with a concentration of 72 µg/mL embedded in a tumor, a signal intensity difference of 39% can be observed with normal white matter if a TR value of 500 msec is used. The signal intensity difference between the tumor with particles and normal gray matter will be even greater than 39%. One can select either greater or lower concentrations of particles, depending on the desired contrast and the surrounding normal tissue (if the surrounding tissue is primarily gray matter or white matter). If concentrations as low as 47 µg/mL are used, the following signal intensity can be observed:

$$\%\ Difference = \frac{0.45 - 0.38}{0.38} * 100 = 18\%$$

Equation 9: Percentage of signal intensity difference between normal white matter and a tumor with a concentration of 14.4nm particles of 47 µg/mL

Even at a concentration of 72 µg/mL , 32.4nm do not provide a high enough relaxation rate in order to keep the signal above the normal white and gray matter. It is expected that there would be no contrast between normal brain matter and a tumor with particles of 32.4nm, unless extremely, unfeasibly high concentrations are used. The following image display the T_1 relaxation analysis for 32.4nm particles embedded in the tumor at the same concentrations used in the previous analysis of 14.4nm.

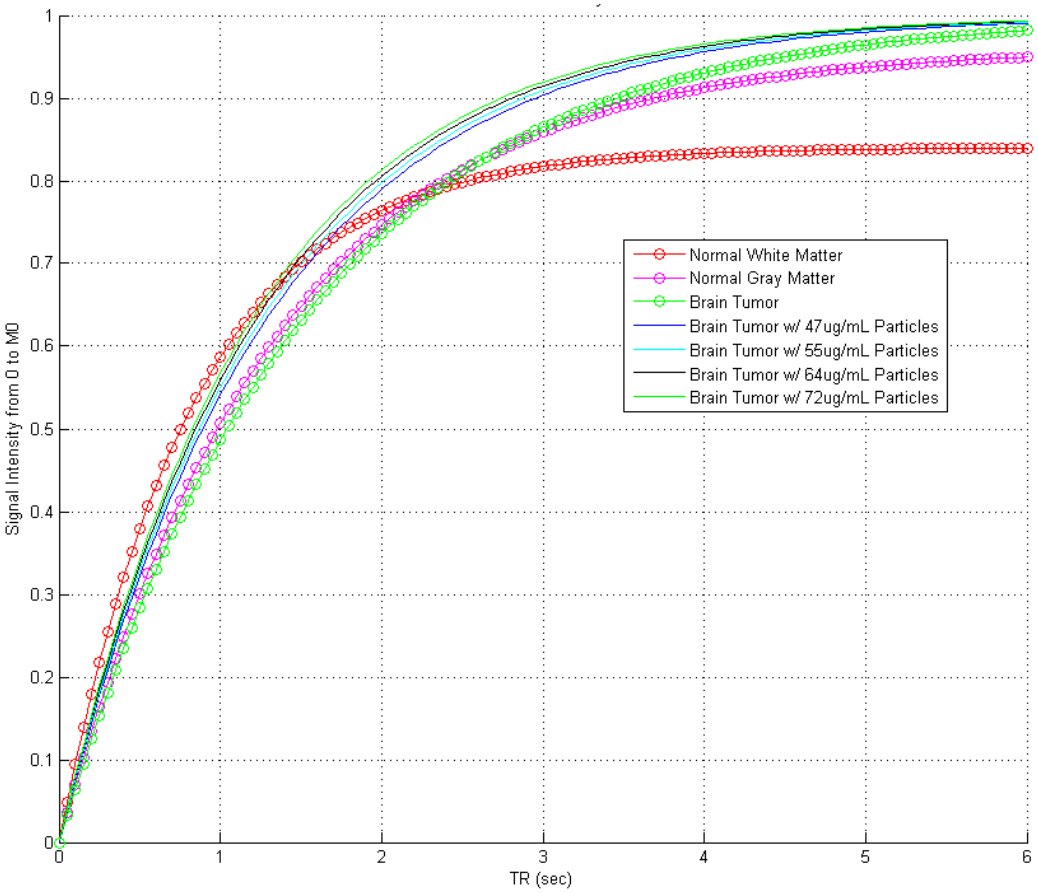

Figure 24: T_1 relaxation analysis for normal white and gray matter, a typical brain tumor, and brain tumor with 32.4nm particles of varying concentrations.

The plot above shows that a brain tumor with embedded 32.4nm particles at concentrations between 47 and 72 µg/mL does not provide any contrast enhancement. In fact, most of the signal of the tumor with embedded particles lies in the region of the normal white and gray matter. From an imaging perspective, it would be impossible to differentiate between the tumor and normal tissue. Extremely high concentrations around 300 µg/mL could be used in order to achieve similar contrast enhancement to which 14.4nm particles provide. However, the T_2 signal would be completely attenuated at low TE values, and thus there is very little usable application of 32.4nm particles.

The iron-oxide nanoparticles can also be used as T_2 contrast agents. In fact, super-paramagnetic iron-oxide particles have been known for their substantial impact on T_2-weighted images. T_2 relaxation curves were plotted for both normal white and gray matter, as well as a typical tumor. Additionally, the curves for tumors with particles at different concentrations and particle sizes were plotted as shown in Figure 25.

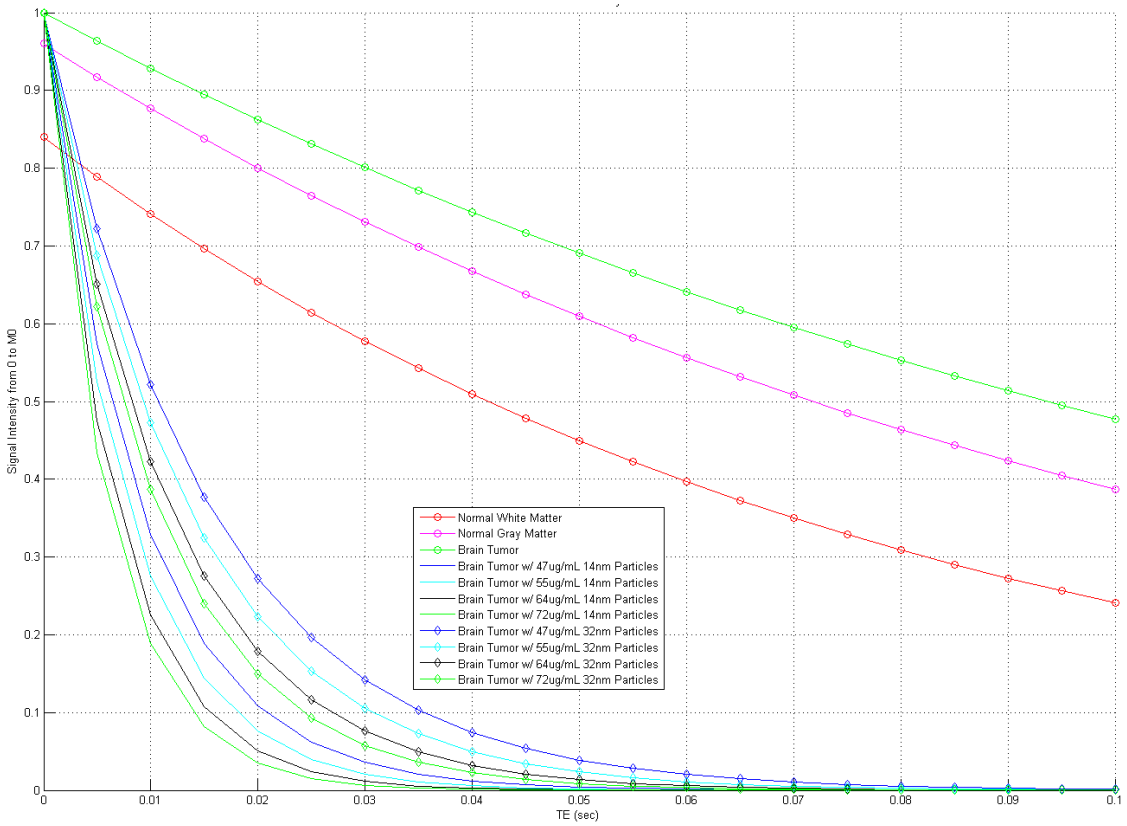

Figure 25: T_2 relaxation analysis (signal intensity as a function of the echo time TE) for normal white and gray matter, a typical brain tumor, and tumor with particles of varying concentrations and sizes.

The equation used for T_2 relaxation analysis is the following:

$$M_{xy}(TE) = M_0 * e^{-TE/T_2}$$

Equation 10

For T_2-weighted images, long TE and long TR times are typically used. However, when using T_2 relaxation agents such as iron-particles, shorter TE values are needed in order to maintain a good signal-to-noise ratio (SNR). Under normal operating conditions, on clinical MRI instruments, about the shortest TE value that is possible with currently technology is around 8 msec. Iron particles have the capability of attenuating the signal substantially, however, in order to maintain good SNR, it is desired to obtain MRI data where the signal intensity of the tumor with particles is above 25% of M_0. Equation 10 can be used to calculate the required T_2 relaxation time in order to meet the parameters of $0.25M_0$ with a TE of 8

msec. With these parameters, a T_2 relaxation time of about 0.006 seconds is required. Figure 22 can then be referenced in order to determine the desired particle concentration of 14.4nm particles for this T_2 value or R_2 value of 167 $msec^{-1}$(1/0.006=167). One can see that a concentration of 14.4nm particles around 72 µg/mL will provide a relaxation rate of around 167 $msec^{-1}$. As a comparison, normal white matter has a signal intensity of around 75% of M_0 at TE of 8 msec. Using Equation 7, the percentage of difference of contrast comes out to be 74%, showing that the tumor with particles comes out to be 74% darker than the normal white matter when using a concentration of 72 µg/mL of 14.4nm. Therefore, using particles at this concentration makes an excellent T_2 contrast agent.

$$\%\ Difference = \left|\frac{0.19 - 0.74}{0.74}\right| * 100 = 74\%$$

Equation 11: Percentage of signal intensity difference between normal white matter and a tumor with a concentration of 14.4nm particles of 72 µg/mL

Additionally, if 32.4nm particles are used at 47 µg/mL, the signal intensity difference will be around 30%, which is still significant contrast. This calculation is shown below.

$$\%\ Difference = \left|\frac{0.52 - 0.74}{0.74}\right| * 100 = 30\%$$

Equation 12: Percentage of signal intensity difference between normal white matter and a tumor with a concentration of 32.4nm particles of 47 µg/mL

All of the plots in this previous section were created with MATLAB, the code is available in Appendix B.

V. Finalized Design and Conclusion

1. Discussion

i. Health and Safety

Iron is a substance found normally in the bloodstream, and the human body has little difficulty clearing excess amounts. A study in rats[21] has shown that after one hour of intravenous administration, about 82% of the dose was found in the liver, and 6% was found in the spleen. Peak concentrations of iron were found in the liver at 2 hours, and peak concentrations of iron were found in the spleen at 4 hours. This suggests that iron is shifted from the liver to spleen over time. In this study, all of the iron was cleared from the liver within 6 days, and the remaining iron was cleared from the spleen within 8 days from the time of administration (an additional 2 days after fully cleared by the liver). In the conceptual design, MR imaging will be used to confirm the localization of the particles within the tumor. Application of the AMF will not commence until it is confirmed that all particles have either been taken up by the tumor, or cleared by the blood's filtration organs. Undesirable heating of particles in other locations of the body will be avoided by having a waiting period between the intravenous injection and the application of an AMF. It is important to note that the concentration of iron-oxide particles in the previously discussed study was 30 mg of iron per Kg of body weight (the iron in this case was being used to treat anemia). With much smaller concentrations, the waiting time between administration and AMF application is expected to be much shorter.

Another subject of health concern is the safety of the exposure to an alternating current magnetic field. A study[22] showed that if the product of the frequency and amplitude of the magnetic field remains under 4.85×10^8 A/ms, undesirable neural stimulation or heating can be avoided. It may also prove to be desirable, in future modifications, for the magnetic field to be concentrated locally over a particular body part by making use of a surface coil. This would minimize systemic exposure and further minimize any safety concerns.

Lastly, there may be health concerns with the imaging and temperature monitoring methods. Imaging methods such as computed tomography, positron emission tomography, and ultrasound expose the patient to forms of radiation. However, MRI uses magnet fields for imaging and thus do not pose any health concerns. There only lies risk with MRI if the patient has magnetic implants, which may be dislodged during imaging.

ii. Manufacturability

In the design process, it is important to consider manufacturability of the product. To be able to manufacture this design, it is important to make sure that there are no metallic materials used in the MRI and AMF device. It is also important to avoid any interference in the AC current. Lastly, one must consider the process of manufacturing the MRI/AMF device along with the iron oxide nanoparticles to minimize cost and time.

iii. Sustainability

This device should allow for sustainability. The device will be used for a very long time, and if possible, the material used in all parts of the design will be recyclable. The design of the device will also allow for easy maintenance and repair to allow for longer use.

iv. Environmental Impact

The only potential environmental impact involved in this design is the potential of using materials that cannot be recycled after it is no longer in use.

v. Societal Influence

The primary societal influence that may arise from this design is a decrease in fatalities associated with cancer. In 2008, over 560,000 people died of cancer in the United States alone[23] If this device can kill cancerous tumor cells without killing healthy cells, there is great potential in successful ablation of tumors and minimal systemic side effects, thus resulting in a decrease in fatalities from cancer.

vi. Ethical Concerns

There are no particular ethical concerns associated with this design. The only potential concern is for those who do not believe in the introduction of foreign materials into one's body. The introduction of iron oxide nanoparticles into the blood stream may cause concern with certain individuals.

vii. Political Influence

A potential political influence of the design is if it is very successful, there will be a great demand for it. Considering that it will cost a lot of money to manufacture and run this device, there may be a demand for government funding for those who cannot afford it.

viii. Economics

This design can contribute to every day economics in that its production will give jobs to chemists to produce the particles and electrical and biomedical engineers to produce the MRI and AMF portions of the design as well as technicians to run and maintain the device. This device will be quite costly, however if it successfully and efficiently treats cancer, it will be greatly needed. This may result in a need for government funds to make this treatment available to those in great need, otherwise; only people with very high incomes or good insurance can receive the treatment.

2. Conclusion

Throughout the experimental results, the optimum concentrations for MRI contrast enhancement were found. When used as a T_1 contrast agent, the signal intensity difference between tumor tissue with embedded particles and normal white matter is expected to be between 18% and 39% for 14.4nm particles between 47 µg/mL and 72 µg/mL, respectively. When used as a T_2 contrast agent, the signal intensity difference between tumor tissue with embedded particles and normal white matter is expected to be between 30% and 75% for 32.4nm particles at 47 µg/mL and 14.4nm particles at 72 µg/mL. For hyperthermia application, the results of the literature search found the optimal AMF parameters to be a frequency between 80 and 150 KHz, with amplitude between 30 and 86 kA/m. However, these parameters are for the use of concentrations much greater than the range of 47-72 µg/mL; on the magnitude of 3-10 mg/mL. In order to optimize heating for much smaller concentrations of iron, it may be necessary to use much higher frequencies and amplitudes. Higher frequencies will allow more efficient coupling between the particles and the AMF device itself. Higher amplitudes will allow for greater energy delivery and increase temperature. Another factor affecting final temperature that can be achieved is exposure time to the AMF. In the literature, it was found that the parameters discussed earlier were used for times between 5 and 30 minutes. With higher concentrations, the temperature increase over time is more rapid. With smaller concentrations, the temperature increase over time is more gradual. Therefore, it is our expectations that with greater exposure time, the same temperatures can be obtained.

The AMF parameters can further be optimized for the specific particle size and coating in the application. By adjusting the size of the particles, different concentrations of iron can be obtained with different densities of iron particles. Also, there is a correlation between the particle size and the appropriate frequency that must be used. Evidence suggests that with small particle sizes, a greater AMF frequency is required.

The most effective method for temperature monitoring using MRI was found to be T_1 shift monitoring, due to its moderate sensitivity coupled with fast acquisition time. In conclusion, MNPs have properties that can be used to heat cancerous tumor cells while simultaneously acting as an MRI contrast agent for the monitoring of particle uptake and tumor ablation. Hyperthermia treatment can occur while the remainder of the body, even surrounding tissue, remains at physiological temperature.

VI. References

[1] Joseph P. Hornak, The Basics of MRI (Henietta: Interactive Learning Software, 1996-2008). http://www.cis.rit.edu/htbooks/mri/index.html.

[2] Jerry S.H. Lee, Miqin Zhang Conroy Sun, "Magnetic Nanoparticles in MR Imaging and Drug Deliver," Advanced Drug Delivery Reviews 60.11 (2008): 1252-165.

[3] Jain TK, Richey J, Strand M, Leslie-Pelecky DL, Flask CA, Labhasetwar V. Magnetic nanoparticles with dual functional properties: Drug delivery and magnetic resonance imaging. Biomaterials 2008 Oct-1;29(29):4012-21.

[4] Moroz P, Jones SK, Gray BN. Status of hyperthermia in the treatment of advanced liver cancer. J Surg Oncol 2001 Jan-1;77(4):259.

[5] Dennis CL, Jackson AJ, Borchers JA, Ivkov R, Foreman AR, Hoopes PJ, Strawbridge R, Pierce Z, Goerntiz E, Lau JW, Gruettner C. The influence of magnetic and physiological behaviour on the effectiveness of iron oxide nanoparticles for hyperthermia. Journal of Physics.D : Applied Physics 2008 -;41(13):134020.

[6] Zhao DL, Zhang HL, Zeng XW, Xia QS, Tang JT. Inductive heat property of Fe3O4/polymer composite nanoparticles in an ac magnetic field for localized hyperthermia. Biomedical Materials (Materials for Tissue Engineering and Regenerative Medicine) 2006 Dec-1;1(4):198-201.

[7] Gupta AK, Gupta M. Synthesis and surface engineering of iron oxide nanoparticles for biomedical applications. Biomaterials 2005 Jun-1;26(18):3995-4021.

[8] 2007. Absolute medical equipment. <http://www.absolutemed.com/Medical-Equipment/Ultrasound-Machines>. Accessed 2009 Feb 9.

[9] NATORI M. Ultrasound safety: Overview and what we do need in daily clinics for a safe use of diagnostic ultrasound. Int Congr Ser 2004 Oct-1;1274(5):125-8.

[10] 2007. Absolute medical equipment. <http://www.absolutemed.com/Medical-Equipment/CT-Scanners-Systems>. Accessed 2009 Feb 9.

[11] Lockwood D, Einstein D, Davros W. Diagnostic Imaging: Radiation Dose and Patients' Concerns, Journal of Radiology Nursing, Volume 26, Issue 4, December 2007, Pages 121-124, ISSN 1546-0843, DOI: 10.1016/j.jradnu.2007.09.005.

[12] Modified 2008 Aug 22. Industry Canada. <http://www.ic.gc.ca/eic/site/mitr-crtim.nsf/eng/hm00286.html>. Accessed 2009 Feb 9.

[13] 2001. <http://www.mrisafety.com/safety_article.asp?subject=144>
Accessed 2009 Feb 9.

[14] Peller M, Reinl HM, Weigel A, Meininger M, Issels RD, Reiser M. T1 relaxation time at 0.2 tesla for monitoring regional hyperthermia: Feasibility study in muscle and adipose tissue. Magnetic Resonance in Medicine : Official Journal of the Society of Magnetic Resonance in Medicine 2002 Jun-1;47(6):1194-201.

[15] Rieke V., Butts Pauly K. MR thermometry. Journal of Magnetic Resonance Imaging: JMRI 2008 Feb-1;27(2):376-90.

[16] Sun C, Lee JS, Zhang M. Magnetic nanoparticles in MR imaging and drug delivery. Adv Drug Deliv Rev 2008 Aug-17;60(11):1252-65.

[16] Weissleder R, Stark DD, Engelstad BL, Bacon BR, Compton CC, White DL, Jacobs P, Lewis J. Superparamagnetic iron oxide: Pharmacokinetics and toxicity. AJR.American Journal of Roentgenology 1989 Jan-1;152(1):167-73.

[16] Atkinson, W J. Usable frequencies in hyperthermia with thermal seeds. *IEEE Transactions On Biomedical Engineering* Volume: 31 Issue: 1 (1984-01-01) p. 70-75. ISSN: 0018-9294

[17] Wansapura JP, Holland SK, Dunn RS, Ball WS Jr. NMR relaxation times in the human brain at 3.0 tesla. Journal of Magnetic Resonance Imaging : JMRI 1999 Apr-1;9(4):531-8.

[18] Andersen, C. In vivo estimation of water content in cerebral white matter of brain tumour patients and normal individuals: Towards a quantitative brain oedema definition. Acta Neurochir 1997 Jan-1;139(3):249-55.

[19] Tofts P. Quantitative MRI of the brain. John Wiley and Sons; 2003. 650 p.

[20] Kiricuta ICJ, Simplaceanu V. Tissue water content and nuclear magnetic resonance in normal and tumor tissues. Cancer Res 1975 May-1;35(5):1164-7.

[21] Weissleder R, Stark DD, Engelstad BL, Bacon BR, Compton CC, White DL, Jacobs P, Lewis J. Superparamagnetic iron oxide: Pharmacokinetics and toxicity. AJR.American Journal of Roentgenology 1989 Jan-1;152(1):167-73.

[22] Atkinson, W J. Usable frequencies in hyperthermia with thermal seeds. *IEEE Transactions On Biomedical Engineering* Volume: 31 Issue: 1 (1984-01-01) p. 70-75. ISSN: 0018-9294

[23] National Cancer Institute. http://seer.cancer.gov/statfacts/html/all.html. Accessed April 12th, 2009.

Appendix A: Relaxivity Data

14.4nm T1 data	5ug/ml	TI	0.005 0.007 0.009 0.012 0.015 0.02 0.03 0.04 0.05 0.1 0.15 0.2 0.4 0.6 0.8 1 2 3 4 5 6 7 8
		Intesity	-2.36 -2.38 -2.39 -2.39 -2.37 -2.53 -2.46 -2.23 -2.24 -2.16 -2.07 -1.99 -1.66 -1.36 -1.08 -0.83 0.21 0.91 1.38 1.71 2.11 2.28 2.39
	10ug/ml	TI	0.005 0.007 0.009 0.012 0.015 0.02 0.03 0.04 0.05 0.1 0.15 0.2 0.4 0.6 0.8 1 2 3 4 5 6 7 8
		Intesity	-2.15 -2.08 -2.30 -2.28 -2.27 -2.26 -2.21 -2.16 -2.13 -2.03 -1.93 -1.85 -1.49 -1.18 -0.88 -0.62 0.41 1.08 1.51 1.79 1.97 2.09 2.17
	20ug/ml	TI	0.007 0.009 0.012 0.015 0.02 0.03 0.04 0.05 0.1 0.15 0.2 0.4 0.6 0.8 1 2 3 4 5 6 7 8
		Intesity	-2.53 -2.51 -2.50 -2.48 -2.44 -2.40 -2.37 -2.35 -2.21 -2.09 -1.96 -1.49 -1.07 -0.7 -0.36 0.87 1.58 1.99 2.23 2.37 2.45 2.50
	30ug/ml	TI	0.005 0.007 0.009 0.012 0.015 0.02 0.03 0.04 0.05 0.1 0.15 0.2 0.4 0.6 0.8 1 2 3 4 5 6 7 8
		Intesity	-2.05 -2.17 -2.16 -2.15 -2.01 -2.00 -1.97 -1.94 -1.92 -1.78 -1.65 -1.58 -1.07 -0.71 -0.34 0.02 1.09 1.66 1.95 2.11 2.19 2.24 2.26
	50ug/ml	TI	0.005 0.007 0.009 0.012 0.015 0.02 0.03 0.04 0.05 0.1 0.15 0.2 0.4 0.6 0.8 1 2 3 4 5 6 7 8
		Intesity	-2.27 -2.26 -2.26 -2.24 -2.21 -2.20 -2.15 -2.11 -2.07 -1.87 -1.67 -1.59 -0.83 -0.29 0.17 0.56 1.71 2.18 2.39 2.46 2.50 2.52 2.53
14.4nm T2 Data	5ug/ml	TE	0.012 0.014 0.015 0.02 0.025 0.03 0.035 0.04 0.045 0.05 0.06 0.07 0.08 0.09 0.1 0.12 0.16 0.2 0.24 0.28 0.32 0.36 0.4 0.45
		Intesity	7.60 7.48 7.38 7.07 6.74 6.30 5.9 5.52 5.19 4.91 4.41 3.85 3.39 3.01 2.64 2.05 1.19 0.68 0.38 0.19 0.11 0.06 0.03 0.01
	10ug/ml	TE	0.012 0.014 0.015 0.02 0.025 0.03 0.035 0.04 0.045 0.05 0.06 0.07 0.08 0.09 0.1 0.12 0.16 0.2 0.24 0.28 0.32 0.36 0.4 0.45
		Intesity	5.72 5.50 5.38 4.86 4.33 3.81 3.37 2.99 2.67 2.37 1.85 1.46 1.15 0.9 0.71 0.43 0.16 0.06 0.02 0.01 0.00 0.00 0.00 0.00
	20ug/ml	TE	0.012 0.014 0.015 0.02 0.025 0.03 0.035 0.04 0.045 0.05 0.06 0.07 0.08 0.09 0.1 0.12 0.2 0.24 0.28 0.32 0.36 0.4 0.45
		Intesity	4.66 4.31 4.12 3.31 2.59 2.17 1.73 1.39 1.09 0.86 0.54 0.34 0.21 0.13 0.08 0.03 0.0 0.0 0.0 0.00 0.00 0.00 0.00
	30ug/ml	TE	0.0120 0.0125 0.0130 0.0135 0.0140 0.0145 0.0150 0.0155 0.0160 0.0165 0.0175 0.020 0.025 0.030 0.035 0.040 0.045 0.050 0.06 0.07 0.08 0.09 0.1 0.2 0.3 0.4
		Intesity	6.10 5.91 5.68 5.52 5.31 5.13 4.95 4.79 4.62 4.24 3.93 3.46 2.4 1.67 1.16 0.8 0.55 0.39 0.18 0.09 0.04 0.02 0.01 0.0 0.0 0.0
	50ug/ml	TE	0.0120 0.0125 0.0130 0.0135 0.0140 0.0145 0.0150 0.0155 0.0160 0.0165 0.017 0.0175 0.018 0.020 0.025 0.030 0.035 0.040 0.045 0.050 0.06 0.07 0.08 0.09 0.1 0.2 0.3 0.4
		Intesity	4.13 3.88 3.69 3.48 3.29 3.14 2.95 2.80 2.66 2.51 2.37 2.25 2.14 1.7 0.98 0.56 0.32 0.18 0.1 0.06 0.02 0.01 0.0 0.0 0.0 0 0 0
32.4nm T1 data	5ug/ml	TI	0.005 0.007 0.009 0.012 0.015 0.02 0.04 0.1 0.15 0.2 0.4 0.6 0.8 1 2 3 4 5 6 7 8
		Intesity	-2.12 -2.11 -2.10 -2.10 -2.11 -2.13 -2.09 -1.98 -1.90 -1.85 -1.57 -1.30 -0.96 -0.74 0.13 0.74 1.16 1.45 1.66 1.8 1.9
	10ug/ml	TI	0.005 0.007 0.009 0.012 0.015 0.05 0.1 0.15 0.2 0.4 0.6 0.8 1 2 3 4 5 6 7 8
		Intesity	-1.92 -1.90 -1.89 -1.88 -1.91 -1.9 -1.83 -1.76 -1.68 -1.41 -1.16 -0.92 -0.70 0.18 0.79 1.22 1.5 1.55 1.68 1.77
	20ug/ml	TI	0.005 0.007 0.009 0.012 0.015 0.02 0.03 0.04 0.05 0.1 0.15 0.2 0.8 1 2 4 5 6 7 8
		Intesity	-2.11 -2.10 -2.11 -2.29 -2.31 -2.33 -2.13 -2.08 -2.06 -1.99 -1.91 -1.82 -0.92 -0.66 0.35 1.48 1.78 1.98 2.12 2.21
	30ug/ml	TI	0.005 0.007 0.009 0.012 0.015 0.02 0.03 0.04 0.05 0.1 0.15 0.2 0.4 0.6 0.8 1 2 4 5 6 7 8
		Intesity	-2.03 -2.01 -1.99 -2.01 -2.01 -2.03 -1.86 -2.02 -2.01 -1.92 -1.82 -1.73 -1.4 -1.09 -0.81 -0.55 0.46 1.53 1.81 1.98 2.10 2.18
	50ug/ml	TI	0.005 0.007 0.009 0.012 0.015 0.02 0.03 0.04 0.05 0.1 0.15 0.2 0.4 0.6 1 3 4 5 6 7 8
		Intesity	-1.98 -1.98 -2.00 -2.00 -2.0 -1.99 -1.96 -1.93 -1.92 -1.81 -1.71 -1.61 -1.23 -0.89 -0.31 1.36 1.73 1.96 2.1 2.19 2.24
32.4nm T2 Data	5ug/ml	TE	0.012 0.014 0.015 0.02 0.025 0.03 0.035 0.04 0.045 0.05 0.06 0.07 0.08 0.09 0.1 0.12 0.16 0.2 0.24 0.28 0.32 0.36 0.4 0.45
		Intesity	7.68 7.57 7.51 7.25 6.99 6.75 6.51 6.27 6.06 5.76 5.45 5.08 4.65 4.4 4.09 3.48 2.59 1.93 1.39 1.01 0.73 0.52 0.38 0.24
	10ug/ml	TE	0.012 0.014 0.015 0.02 0.025 0.03 0.035 0.04 0.045 0.05 0.06 0.07 0.08 0.09 0.1 0.12 0.16 0.2 0.24 0.28 0.32 0.36 0.4 0.45
		Intesity	7.55 7.31 7.19 6.63 6.09 5.59 5.14 4.71 4.33 3.96 3.35 2.83 2.39 2.00 1.69 1.20 0.59 0.29 0.14 0.07 0.03 0.01 0.00 0.00
	20ug/ml	TE	0.012 0.014 0.015 0.02 0.025 0.03 0.035 0.04 0.045 0.05 0.06 0.07 0.08 0.09 0.1 0.12 0.16 0.2 0.24 0.28 0.32 0.36 0.4 0.45
		Intesity	6.79 6.47 6.29 5.52 4.84 4.24 3.71 3.25 2.84 2.49 1.91 1.46 1.12 0.85 0.65 0.38 0.13 0.04 0.02 0.00 0.00 0.00 0.00 0.00
	30ug/ml	TE	0.0120 0.0125 0.0130 0.0135 0.0140 0.0145 0.0150 0.0155 0.0160 0.0165 0.0175 0.020 0.025 0.030 0.035 0.040 0.045 0.050 0.06 0.07 0.08 0.09 0.1 0.2 0.3 0.4
		Intesity	6.52 6.52 6.4 6.30 6.05 6.05 5.82 5.70 5.6 5.48 5.26 5.12 4.25 3.5 2.89 2.38 1.97 1.62 1.11 0.75 0.51 0.35 0.24 0.0 0.0 0.0
	50ug/ml	TE	0.0120 0.0125 0.0130 0.0135 0.0140 0.0145 0.0150 0.0155 0.0160 0.0165 0.017 0.0175 0.018 0.020 0.025 0.030 0.035 0.040 0.045 0.050 0.06 0.07 0.08 0.09 0.1 0.2 0.3 0.4
		Intesity	1.75 1.68 1.63 1.58 1.52 1.47 1.43 1.38 1.34 1.29 1.26 1.21 1.17 1.03 0.75 0.55 0.4 0.29 0.21 0.15 0.08 0.04 0.02 0.01 0.01 0.0 0 0

Appendix B: MATLAB Code

Effects of Iron Particles on Tumors

```
%% EFFECTS OF IRON PARTICLES ON TUMORS
%T1 of Tumor in Seconds
T1tumor=1.500;
%T2 of Tumor in Seconds
T2tumor=0.135;

R1tumor=1/T1tumor;
R2tumor=1/T2tumor;

% Concentrations used in ug/mL
Conc=[0 5 10 20 30 50 70 90];

%R1 for 14.4nm
subplot(2,2,1)
grid on
hold on
R1initial1=0.0115*Conc+0.3156; %Eq. taken from fitted data, particles alone
plot(Conc,R1initial1,'r')
R1final1=0.0115*Conc+R1tumor; %Eq. for tumor with particles
plot(Conc,R1final1,'b');
xlabel('Concentration (ug/mL)')
ylabel('R1 (1/sec)')
title('R1 Values for Tumor With 14.4nm Particles')
legend('Iron-oxide Particles in Solution','Iron-oxide Particles in Tumor',
'Location','SouthEast')

%R1 for 32.4nm
hold off
subplot(2,2,2)
grid on
hold on
R1initial2=0.0024*Conc+0.3655;
plot(Conc,R1initial2,'r');
R1final2=0.0024*Conc+R1tumor;
plot(Conc,R1final2,'b');
xlabel('Concentration (ug/mL)')
ylabel('R1 (1/sec)')
title('R1 Values for Tumor With 32.4nm Particles')
legend('Iron-oxide Particles in Solution','Iron-oxide Particles in Tumor',
'Location','SouthEast')

%R2 for 14.4nm
hold off
subplot(2,2,3)
grid on
hold on
R2initial1=2.2107*Conc+1.765;
plot(Conc,R2initial1,'r');
R2final1=2.2107*Conc+R2tumor;
```

```
plot(Conc,R2final1,'b');
xlabel('Concentration (ug/mL)')
ylabel('R2 (1/sec)')
title('R2 Values for Tumor With 14.4nm Particles')
legend('Iron-oxide Particles in Solution','Iron-oxide Particles in Tumor',
'Location','SouthEast')

%R2 for 32.4nm
hold off
subplot(2,2,4)
grid on
hold on
R2initial2=1.2201*Conc+2.2635;
plot(Conc,R2initial2,'r');
R2final2=1.2201*Conc+R2tumor;
plot(Conc,R2final2,'b');
xlabel('Concentration (ug/mL)')
ylabel('R2 (1/sec)')
title('R2 Values for Tumor With 32.4nm Particles')
legend('Iron-oxide Particles in Solution','Iron-oxide Particles in Tumor',
'Location','SouthEast')
```

T1 Relaxation Curves for Normal White Matter and Brain w/ Particles at 3.0T

```
Hold on
%% T1 Relaxation Curves for Normal White Matter and Brain w/ Particles at
3.0T
% R1 of Tumor with 14.4nm Particles
R1p47=1.2;
R1p55=1.3;
R1p64=1.4;
R1p72=2.5;
T1p47=1/R1p47;
T1p55=1/R1p55;
T1p64=1/R1p64;
T1p72=1/R1p72;

% 3.0 Tesla Magnet Normalized from 0 to 1 signal intensity
M0=1;

% "a" Determined from Modeled Data
a=1;

%Time vector
TR=0:0.05:6;

% Normal White Matter (T1=832msec)
Mz1=(0.84*M0)*(1-a*exp(-TR/0.832));
plot(TR,Mz1,'ro-')
```

```
% Normal Gray Matter (T1=1331msec)
Mz1=(0.96*M0)*(1-a*exp(-TR/1.331));
plot(TR,Mz1,'mo-')

% Brain Tumor (T1=1500msecESTIMATE)
Mz2=M0*(1-a*exp(-TR/1.500));
plot(TR,Mz2,'go-')

% Brain Tumor w/ Particles @ 47ug/mL
Mz3=M0*(1-a*exp(-TR/T1p47));
plot(TR,Mz3,'b')

% Brain Tumor w/ Particles @ 55ug/mL
Mz3=M0*(1-a*exp(-TR/T1p55));
plot(TR,Mz3,'c')

% Brain Tumor w/ Particles @ 64ug/mL
Mz3=M0*(1-a*exp(-TR/T1p64));
plot(TR,Mz3,'k')

% Brain Tumor w/ Particles @ 72ug/mL
Mz3=M0*(1-a*exp(-TR/T1p72));
plot(TR,Mz3,'g')


xlabel('TR (sec)')
ylabel('Signal Intensity from 0 to M0')
title('T1 Relaxation Analysis')
legend('Normal White Matter','Normal Gray Matter','Brain Tumor','Brain Tumor
w/ 47ug/mL Particles','Brain Tumor w/ 55ug/mL Particles','Brain Tumor w/
64ug/mL Particles','Brain Tumor w/ 72ug/mL Particles','Location','Best')



%% T2 Relaxation Curves for Normal White Matter and Brain w/ Particles at
3.0T

%R2 of Tumor with 14.4nm Particles
R2p47=111;
R2p55=129;
R2p64=149;
R2p72=167;
T2p47=1/R2p47;
T2p55=1/R2p55;
T2p64=1/R2p64;
T2p72=1/R2p72;

grid on
hold off
figure(2)
grid on
hold on
```

```
% Time vector
TE=0:0.005:.1;

% Normal White Matter(T2=80msec)
Mz1b=0.84*M0*exp(-TE/0.080);
plot(TE,Mz1b,'ro-')

% Normal Gray Matter(T2=110msec)
Mz1b=0.96*M0*exp(-TE/0.110);
plot(TE,Mz1b,'mo-')

% Brain Tumor (T2=135msecESTIMATE)
Mz2b=M0*exp(-TE/0.135);
plot(TE,Mz2b,'go-')

% Brain Tumor w/ 47ug/mL 14nm Particles
Mz3b=M0*exp(-TE/T2p47);
plot(TE,Mz3b,'b')

% Brain Tumor w/ 55ug/mL 14nm Particles
Mz3b=M0*exp(-TE/T2p55);
plot(TE,Mz3b,'c')

% Brain Tumor w/ 64ug/mL 14nm Particles
Mz3b=M0*exp(-TE/T2p64);
plot(TE,Mz3b,'k')

% Brain Tumor w/ 72ug/mL 14nm Particles
Mz3b=M0*exp(-TE/T2p72);
plot(TE,Mz3b,'g')


% R2 of Tumor with 32.4nm Particles
R2p47b=65;
R2p55b=75;
R2p64b=86;
R2p72b=95;
T2p47b=1/R2p47b;
T2p55b=1/R2p55b;
T2p64b=1/R2p64b;
T2p72b=1/R2p72b;

% Brain Tumor w/ 47ug/mL 32nm Particles
Mz3b=M0*exp(-TE/T2p47b);
plot(TE,Mz3b,'bd-')

% Brain Tumor w/ 55ug/mL 32nm Particles
Mz3b=M0*exp(-TE/T2p55b);
plot(TE,Mz3b,'cd-')

% Brain Tumor w/ 64ug/mL 32nm Particles
Mz3b=M0*exp(-TE/T2p64b);
plot(TE,Mz3b,'kd-')
```

```
% Brain Tumor w/ 72ug/mL 32nm Particles
Mz3b=M0*exp(-TE/T2p72b);
plot(TE,Mz3b,'gd-')

xlabel('TE (sec)')
ylabel('Signal Intensity from 0 to M0')
title('T2 Relaxation Analysis')
legend('Normal White Matter','Normal Gray Matter','Brain Tumor','Brain Tumor
w/ 47ug/mL 14nm Particles','Brain Tumor w/ 55ug/mL 14nm Particles','Brain
Tumor w/ 64ug/mL 14nm Particles','Brain Tumor w/ 72ug/mL 14nm
Particles','Brain Tumor w/ 47ug/mL 32nm Particles','Brain Tumor w/ 55ug/mL
32nm Particles','Brain Tumor w/ 64ug/mL 32nm Particles','Brain Tumor w/
72ug/mL 32nm Particles','Location','Best')
```